LETTER Communicated by Bard Ermentrout

Effects of Noisy Drive on Rhythms in Networks of Excitatory and Inhibitory Neurons

Christoph Börgers
christoph.borgers@tufts.edu
Department of Mathematics, Tufts University, Medford, MA 02155, U.S.A.

Nancy Kopell
nk@math.bu.eds
Department of Mathematics and Center for BioDynamics, Boston University, Boston, MA 02215, U.S.A.

Synchronous rhythmic spiking in neuronal networks can be brought about by the interaction between E-cells and Icells (excitatory and inhibitory cells). The I-cells gate and synchronize the E-cells, and the E-cells drive and synchronize the I-cells. We refer to rhythms generated in this way as PING (pyramidal-interneuronal gamma) rhythms. The PING mechanism requires that the drive I_I to the I-cells be sufficiently low; the rhythm is lost when I_I gets too large. This can happen in at least two ways. In the first mechanism, the I-cells spike in synchrony, but get ahead of the E-cells, spiking without being prompted by the E-cells. We call this *phase walkthrough of the I-cells*. **In the second mechanism, the I-cells fail to synchronize, and their activity leads to complete suppression of the E-cells. Noisy spiking in the E-cells, generated by noisy external drive, adds excitatory drive to the I-cells and may lead to phase walkthrough. Noisy spiking in the I-cells adds inhibition to the E-cells and may lead to suppression of the E-cells. An analysis of the conditions under which noise leads to phase walkthrough of the I-cells or suppression of the E-cells shows that PING rhythms at frequencies far below the gamma range are robust to noise only if network parameter values are tuned very carefully. Together with an argument explaining why the PING mechanism does not work far above the gamma range in the presence of heterogeneity, this justifies the "G" in "PING."**

1 Introduction

The gamma rhythm, a 30 to 80 Hz rhythm in the nervous system, has been associated with early sensory processing (Singer & Gray, 1995; Fries, Neuenschwander, Engel, Goebel, & Singer, 2001; Fries, Roelfsema, Engel, König, & Singer, 1997), attention (Tiitinen et al., 1993; Pulvermüller, Birbaumer, Lutzenberger, & Mohr, 1997), and memory (Tallon-Baudry, Bertrand, Per-

onnet, & Pernier, 1998; Slotnick, Moo, Kraut, Lesser, & Hart, 2002). It has also been associated with the formation of cell assemblies, that is, temporarily synchronous sets of cells that work together in some aspect (Engel, König, Kreiter, Schillen, & Singer, 1992; Singer & Gray, 1995; Singer, 1999; Olufsen, Whittington, Camperi, & Kopell, 2003). However, it is still not completely understood which mechanisms underlie gamma rhythms, which biophysical parameters are important in these mechanisms, and how gamma rhythms participate in the formation of cell assemblies.

Several different kinds of gamma rhythms have been observed in vivo, in vitro, and in computational studies. Synchronization may result from chemical synapses between inhibitory cells (Whittington, Traub, & Jefferys, 1995; Traub, Whittington, Colling, Buzsáki, & Jefferys, 1996; Wang & Buzsáki, 1996; Whittington, Traub, Kopell, Ermentrout, & Buhl, 2000; Tiesinga, Fellous, José, & Sejnowski, 2001; Hansel & Mato, 2003). Gamma rhythms generated in this way have been called interneuronal gamma (ING) rhythms (Whittington, et al., 2000) or γ-I rhythms (Tiesinga et al., 2001). The mechanism has also been called the mutual inhibition mechanism by Hansel and Mato (2003). In this letter, we study gamma rhythms resulting from chemical synapses between excitatory (pyramidal) cells and inhibitory cells. The I-cells (inhibitory cells) gate and synchronize the E-cells (excitatory cells), and the E-cells drive and synchronize the I-cells (Whittington et al., 2000; Tiesinga et al., 2001; Hansel & Mato, 2003). Gamma rhythms of this kind have been called pyramidal-interneuronal gamma (PING) rhythms (Whittington et al., 2000) or γ-II rhythms (Tiesinga et al., 2001). The mechanism has also been called the cross-talk mechanism by Hansel and Mato (2003)[1] In vitro, PING is produced by tetanic stimulation (Whittington et al., 2000). PING is believed to be associated with the creation of cell assemblies (Whittington et al., 2000; Olufsen et al., 2003).

Other mechanisms, not modeled here, are believed to play a role in the generation of at least some gamma rhythms. Electrical coupling between dendrites of interneurons can contribute to enhancing the coherence of rhythms (Tamás, Buhl, Lörincz, & Somogyi, 2000; Traub et al., 2001). Electrical coupling between axons of pyramidal cells is believed to play a central role in driving persistent gamma oscillations in the CA3 region of the hippocampus (Traub et al., 2000). Chattering cells, which intrinsically generate bursts of action potentials at gamma frequency, play a role in generating some gamma rhythms (Gray & McCormick, 1996; Traub, Buhl, Golveli, & Whittington, 2003).

Unlike these forms of gamma, PING can be captured by models that abstract from much of the biophysical detail. In general, pyramidal cells are capable of producing many ionic currents. However, some currents that are not involved in producing action potentials, such as I_h and I_T, are negligible

[1] PING is one of two "cross-talk mechanisms" discussed by Hansel and Mato (2003).

during PING activity, since the voltage does not become sufficiently low during any part of the cycle. Other currents, such as, slow outward potassium currents, are weakened by the large activation of metabotropic glutamate receptors needed to produce PING (Storm, 1989; Charpak, Gähwiler, Do, & Knöpfel, 1990; Whittington et al., 2000). Consequently, during PING, the electrophysiological behavior is well described by standard Hodgkin-Huxley equations, which can often be well approximated by reduced equations such as the quadratic integrate-and-fire model (Latham, Richmond, Nelson, & Nirenberg, 2000) and the theta model (Ermentrout & Kopell, 1986; Hoppensteadt & Izhikevich, 1997; Gutkin & Ermentrout, 1998). These reductions and relevant parameter regimes are described in section 2.

It is easy to describe and understand the PING mechanism in a network consisting of just one E-cell and one I-cell. The E-cell fires and excites the I-cell enough to fire. The I-cell fires and temporarily inhibits the E-cell. This simple mechanism, discussed in more detail in section 3, requires that external excitatory drive to the I-cell be sufficiently weak that the I-cell fires only in response to the E-cell, not on its own. When this condition is violated, phase walkthrough of the I-cell occurs, that is, the I-cell does not wait for input from the E-cell to fire, destroying the regular rhythm.[2] The region in parameter space in which phase walkthrough occurs is bounded by a hypersurface that we call the phase walkthrough boundary. It is discussed in detail in section 4. Clearly, phase walkthrough of the I-cell occurs more easily when the E-cell is driven less strongly.

The dynamical properties of the rhythm become more subtle when there are large populations of E- and I-cells. The key to the PING rhythm in large networks is the mechanism by which the I-cells synchronize the E-cells. Section 5 gives an explanation of this mechanism. If approximate synchronization is to occur in the presence of heterogeneity, the ratio

$$r = \frac{\text{strength of inhibitory synaptic currents into E-cells}}{\text{strength of excitatory input drive to E-cells}} \tag{1.1}$$

must be sufficiently large (see section 5). (A refined definition of r is given later.)

In a two-cell network, phase walkthrough of the I-cells is the only mechanism by which the PING rhythm can be lost as external drives are varied. In larger networks, there is a second important mechanism: suppression of the E-cells by asynchronous activity of the I-cells. (The I-cells are most effective at suppressing the E-cell when they are asynchronous. See appendix A.) In a simulation in which the I-cells are asynchronous initially and receive strong external drive, suppression of the E-cells may occur immediately, preventing the PING mechanism from synchronizing the network. The region in

[2] Throughout this letter, we take the word *rhythm* to denote a regular rhythm. For instance, the firing pattern in the right panel of Figure 4 is not considered a "rhythm."

parameter space in which asynchronous activity of the I-cells is capable of suppressing the E-cells is bounded by a hypersurface that we call the suppression boundary. It is discussed in detail in section 6. It turns out that the quantity r plays the central role here: suppression occurs more easily for larger r. Bistability between suppression and synchrony is analyzed in section 7.

Our study of the phase walkthrough and suppression boundaries casts light on the behavior of PING rhythms in the presence of noisy external drive. The rhythm may not be disrupted by occasional out-of-order spiking of E-cells, caused by noisy external drive. However, too much noisy spiking of the E-cells generates too much tonic excitatory drive to the I-cell, resulting in phase walkthrough. This is analyzed in section 8. Since phase walkthrough of the I-cells occurs more easily for weaker external drive to the E-cells, PING rhythms are more easily abolished by noisy activity in the E-cells when external drive to the E-cells is weaker; the analysis in section 8 makes this quantitative.

Similarly, the rhythm may not be disrupted by occasional out-of-order spiking of I-cells. However, too much noisy spiking of the I-cells generates too much tonic inhibitory drive to the E-cells, resulting in their suppression. This is analyzed in section 9. Since suppression of the E-cells occurs easily for large values of r, PING rhythms are easily abolished by noisy activity in the I-cells when r is large.

The analysis and most of the simulations presented in this article assume homogeneity in network parameter values and all-to-all connectivity. However, we believe that moderate amounts of heterogeneity and significant sparseness in connectivity do not affect the conclusions. Some simulations, including heterogeneity and sparseness, are presented in section 10.

To lower the frequency of a PING rhythm, one must decrease the external drive I_E to the E-cells or increase r (or both). A decrease in I_E makes phase walkthrough of the I-cells caused by noisy spiking of the E-cells more likely; an increase in r makes the rhythm more susceptible to noise in the I-cells. Our results thus imply that slower PING rhythms are less robust to noise. A PING rhythm will be disrupted by very low levels of noise if its period is many times larger than the decay time constant τ_I of inhibition, that is, if its frequency is far below the gamma range.

If one attempts to raise the frequency above the gamma range (i.e., if one tries to decrease its period below τ_I) by raising I_E, leaving other parameter values unchanged, then r drops, causing the synchronization mechanism to break down, particularly in the presence of heterogeneity. To restore synchronization, one must raise the strength of the I$\rightarrow$E synapses. This brings the frequency back into the gamma range. These arguments are presented in section 11.

In summary, our results justify the "G" in "PING": to be robust in the presence of both heterogeneity and noise, a PING rhythm must have a period that is greater than τ_I, but not many times greater.

2 Networks of Theta Neurons

2.1 The Theta Model. In the theta model, a neuron is represented by a point $P = (\cos\theta, \sin\theta)$ moving on the unit circle S^1. This is analogous to the Hodgkin-Huxley model, which represents a periodically spiking space-clamped neuron by a point moving on a limit cycle in a four-dimensional phase space. In the absence of synaptic coupling, the differential equation describing the motion on S^1 is

$$\frac{d\theta}{dt} = \frac{1-\cos\theta}{\tau} + I\,(1+\cos\theta)\,. \tag{2.1}$$

Here, I should be thought of as an input "current," measured in radians per unit time. The time constant $\tau > 0$ is needed to make equation 2.1 dimensionally correct. Its meaning will be clarified shortly.

For negative I, equation 2.1 has two fixed points, one stable and the other unstable. As I increases, the fixed points approach each other. When $I = 0$, a saddle node bifurcation occurs: the fixed points collide, and cease to exist for positive I.

For a theta neuron, to "spike" means to reach $\theta = \pi$ (modulo 2π), by definition. The transition from $I < 0$ to $I > 0$ is the analog of the transition from excitability to spiking in a neuron.

If $I > 0$ and $-\pi \le \theta_1 \le \theta_2 \le \pi$, the time it takes for θ to rise from θ_1 to θ_2 equals

$$\int_{\theta_1}^{\theta_2} \frac{d\theta}{(1-\cos\theta)/\tau + I(1+\cos\theta)} = \sqrt{\frac{\tau}{I}}\left[\arctan\frac{\tan(\theta/2)}{\sqrt{\tau I}}\right]_{\theta_1}^{\theta_2}. \tag{2.2}$$

Setting $\theta_1 = -\pi$ and $\theta_2 = \pi$ in this formula, we find that the period is

$$T = \pi\sqrt{\frac{\tau}{I}}\,. \tag{2.3}$$

We denote the time it takes for θ to rise from $\pi/2$ to $3\pi/2$ by δ. This should roughly be thought of as the spike duration. Applying formula 2.2 with $(\theta_1, \theta_2) = (\pi/2, \pi)$ and $(\theta_1, \theta_2) = (-\pi, -\pi/2)$ and adding the results, we find

$$\delta = \left[\pi - 2\arctan\frac{1}{\sqrt{\tau I}}\right]\sqrt{\frac{\tau}{I}}\,. \tag{2.4}$$

For physiological realism, we wish to ensure $\delta/T \ll 1$. By equations 2.3 and 2.4,

$$\frac{\delta}{T} = 1 - \frac{2}{\pi}\arctan\frac{1}{\sqrt{\tau I}}\,.$$

Therefore, $\delta/T \ll 1$ means the same as $\tau I \ll 1$. Since $\arctan(1/\epsilon) = \pi/2 - \epsilon + O(\epsilon^2)$ as $\epsilon \to 0$, equation 2.4 implies $\delta \approx 2\tau$ when $\tau I \ll 1$. This reveals the meaning of τ: in the parameter regime of interest to us, τ is approximately half the spike duration. Motivated by this discussion and by the fact that spike durations in real neurons are on the order of milliseconds, we set

$$\tau = 1$$

for the remainder of this article, think of time as measured in milliseconds, and always consider input currents $I \ll 1$. The frequency of a theta neuron is defined to be

$$\nu = \frac{1000}{T}. \tag{2.5}$$

Since we think of t as time measured in milliseconds, ν should be thought of as frequency measured in Hz.

Neuronal models are called of type I if the transition from excitability to spiking involves a saddle node bifurcation on an invariant circle, and of type II if it involves a subcritical Hopf bifurcation (Hodgkin, 1948; Ermentrout, 1996; Gutkin & Ermentrout, 1998; Rinzel & Ermentrout, 1998; Izhikevich, 2000). Thus, the theta model is a type I neuronal model. It is canonical, in the sense that other type I models can be reduced to it by coordinate transformations (Ermentrout & Kopell, 1986; Hoppensteadt & Izhikevich, 1997). In this letter, the E-cells are always modeled as theta neurons. The neuronal model used for the I-cells is irrelevant for many of our arguments; where it matters, we model the I-cells at theta neurons at well.

The theta model can also be derived from the quadratic integrate-and-fire model (Latham et al., 2000)[3]. The general equation of this model is

$$\frac{dV}{dt} = a(V - V_0)(V - V_1) + Q, \tag{2.6}$$

with $a > 0$ and $V_0 < V_1$. After scaling and shifting V and scaling t and Q, equation 2.6 becomes

$$\frac{dV}{dt} = 2V(V - 1) + Q. \tag{2.7}$$

For $Q < 1/2$, equation 2.7 has two fixed points, one stable and the other unstable. As Q increases, the fixed points approach each other. When $Q = 1/2$, a saddle node bifurcation occurs: the fixed points collide and cease

[3] This derivation was shown to us by Rob Clewley, who learned it from Bard Ermentrout.

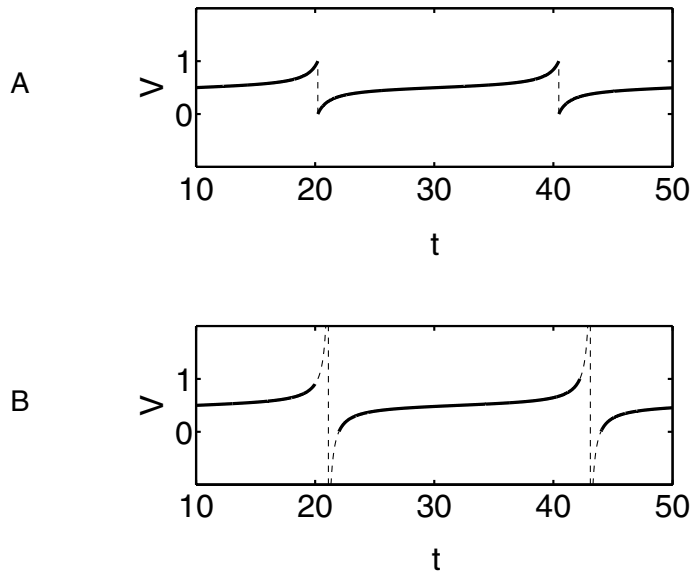

Figure 1: Voltage traces for quadratic integrate-and-fire neuron with (A) threshold at 1 and reset at 0 and (B) threshold at ∞ and reset at $-\infty$.

to exist for positive $Q > 1/2$. We supplement equation 2.7 with the reset condition

$$V(t+0) = 0 \quad \text{if} \quad V(t-0) = 1\,. \tag{2.8}$$

Figure 1A shows V as a function of t for $Q = 0.51$.

The change of variables

$$V = \frac{1}{2} + \frac{1}{2}\tan\frac{\theta}{2} \tag{2.9}$$

transforms equation 2.7 into equation 2.1 with

$$I = \frac{Q - 1/2}{1/2}\,. \tag{2.10}$$

Note that I is the relative deviation of Q from the threshold value $1/2$. The only difference between the quadratic integrate-and-fire model and the theta model lies in the reset condition. The two models are precisely equivalent if equation 2.8 is replaced by

$$V(t+0) = -\infty \quad \text{if} \quad V(t-0) = \infty. \tag{2.11}$$

(Note that V rises from $-\infty$ to ∞ in finite time when $Q > 1/2$.) Figure 1B illustrates the effect of replacing equation 2.8 by 2.11.

2.2 Synapses. The derivation of the theta neuron from the quadratic integrate-and-fire neuron offers a way of modeling conductance-based synapses in the framework of the theta model.[4] One begins by adding a synaptic current to the right-hand side of equation 2.7,

$$\frac{dV}{dt} = -2V(1-V) + Q + gs(V_{rev} - V)\ , \tag{2.12}$$

where g denotes the maximum conductance, $s = s(t) \in [0, 1]$ is a synaptic gating variable (the quantity that the synapse directly acts on), and V_{rev} is the reversal potential of the synapse. For excitatory synapses, V_{rev} should be substantially above the threshold voltage. For inhibitory synapses, it should be somewhat below the reset voltage. We use $V_{rev} = 6.5$ for excitatory synapses and $V_{rev} = -0.25$ for inhibitory synapses throughout this article. Numerical experiments indicate that changes in these values have no qualitative and little quantitative effect on our conclusions. With the change of variables (see equation 2.9), equation 2.12 becomes

$$\frac{d\theta}{dt} = 1 - \cos\theta + \big(I + (2V_{rev} - 1)gs(t)\big)(1 + \cos\theta) - gs(t)\sin\theta\ .$$

Thus, our equation for a theta neuron receiving an excitatory synapse ($V_{rev} = 6.5$) is

$$\frac{d\theta}{dt} = 1 - \cos\theta + \big(I + 12gs(t)\big)(1 + \cos\theta) - gs(t)\sin\theta\ ,$$

and our equation for a theta neuron receiving an inhibitory synapse ($V_{rev} = -0.25$) is

$$\frac{d\theta}{dt} = 1 - \cos\theta + \left(I - \frac{3}{2}gs(t)\right)(1 + \cos\theta) - gs(t)\sin\theta\ . \tag{2.13}$$

For theoretical arguments in this article, we let

$$s(t) = H(t - t_0)e^{-(t-t_0)/\tau_D}\ , \tag{2.14}$$

where t_0 denotes the time of the spike of the presynaptic neuron, H is the Heaviside function,

$$H(t) = \begin{cases} 1 & \text{if } t > 0\ , \\ 0 & \text{if } t \le 0\ , \end{cases} \tag{2.15}$$

[4] This too was shown to us by Rob Clewley, with attribution to Bard Ermentrout.

and $\tau_D > 0$ is the synaptic decay time constant. In numerical simulations of networks of theta neurons, we use a smooth approximation to equation 2.14, defining s to be a solution of the differential equation,

$$\frac{ds}{dt} = -\frac{s}{\tau_D} + e^{-\eta(1+\cos\theta)}\,\frac{1-s}{\tau_R},$$

where θ denotes the dependent variable associated with the presynaptic neuron, $\eta = 5$, and $\tau_R = 0.1$. Thus, s rises rapidly toward 1 when $\theta \approx \pi$ modulo 2π and decays exponentially with time constant τ otherwise.

2.3 Networks of Theta Neurons. The numerical simulations presented in this article are for networks of excitatory and inhibitory theta neurons. Unless stated otherwise, the connectivity is all-to-all, and there is no heterogeneity in network properties. The following notation will be used throughout.

N_E = number of E-cells in the network
N_I = number of I-cells in the network
τ_E = synaptic decay time constant for excitatory synapses
τ_I = synaptic decay time constant for inhibitory synapses
I_E = external drive to E-cells
I_I = external drive to I-cells
g_{IE} = sum of all conductances associated with inhibitory synapses acting on a given E-cell (so an individual $I \to E$ synapse has strength g_{IE}/N_I)
g_{II} = sum of all conductances associated with inhibitory synapses acting on a given I-cell (so an individual $I \to I$ synapse has strength g_{II}/N_I)
g_{EI} = sum of all conductances associated with excitatory synapses acting on a given I-cell (so an individual $E \to I$ synapse has strength g_{EI}/N_E)
g_{EE} = sum of all conductances associated with excitatory synapses acting on a given E-cell (so an individual $E \to E$ synapse has strength g_{EE}/N_E)
T_E = intrinsic period of E-cells $= \pi/\sqrt{I_E}$ (see equation 2.3)
T_I = intrinsic period of I-cells (see section 2.4)
T_P = period of population rhythm
ν_E = intrinsic frequency of E-cells $= 1000/T_E$ (see equation 2.5 and the comment following it)
ν_I = intrinsic frequency of I-cells $= 1000/T_I$
ν_P = frequency of population rhythm $= 1000/T_P$
r = $(3/2)g_{IE}/I_E$

The definition of r given here will, for the remainder of the article, replace the informal definition in equation 1.1. The reason for including the factor $3/2$ in the definition of r will become apparent in section 3.

2.4 Parameter Choices. Unless otherwise stated, we use

$$\tau_E = 2 \quad \text{and} \quad \tau_I = 10$$

in this letter. This is motivated by the decay time constants of excitatory synapses involving AMPA receptors, approximately 2 ms, and inhibitory synapses involving $GABA_A$ receptors, approximately 10 ms. (Recall that we think of t as time in milliseconds.)

As discussed in section 2.1, the external drive I to a theta neuron should be $\ll 1$ for the theta model to be biologically reasonable. We therefore assume that the external drives I_E and I_I are $\ll 1$. An external drive I corresponds to the period $T = \pi/\sqrt{I}$, and therefore to the frequency $\nu = 1000\sqrt{I}/\pi$. For example, $I = 0.1$ corresponds to $\nu \approx 100$, and $I = 0.4$ corresponds to $\nu \approx 200$.

For the PING rhythms studied in this article, it is important that g_{IE} be at least comparable in size to I_E (see section 5). We will often choose $g_{II} = g_{IE}$, but we will also discuss the effects of choosing much smaller values of g_{II}, or even $g_{II} = 0$.

We choose g_{EI} in such a way that a population spike of the E-cells promptly triggers a population spike of the I-cells but does not trigger multiple spikes. If the I-cells are modeled as quadratic integrate-and-fire neurons, the following argument gives a rough indication of how large g_{EI} should be. Consider a network consisting of a single E-cell and a single I-cell. (This is equivalent to a network in which each group of cells, E and I, is fully synchronized.) Recall that $V_{rev} = 6.5$ for excitatory synapses. Since V is near 0 except during spikes, we approximate the term $gs(V_{rev} - V)$ in equation 2.12 by gsV_{rev}. We use the idealized form of s given by equation 2.14. Thus, a spike of the E-cell at time t_0 gives rise to injection of the current $g_{EI}H(t-t_0)e^{-t/\tau_E}V_{rev}$ into the I-cell. Since $\tau_E = 2$ is small in comparison with the periods of the rhythms of interest to us, we introduce the additional approximation that the charge injection resulting from an excitatory synapse is instantaneous, causing a rise in the membrane potential of the I-cell by

$$\Delta V = g_{EI}\tau_E V_{rev} .$$

The excitatory synapse is sure to cause a nearly instantaneous spike of the I-cell if $\Delta V = 1$, that is, if $g_{EI} = 1/(\tau_E V_{rev})$. Since we use $\tau_E = 2$ and $V_{rev} = 6.5$ throughout, this means $g_{EI} = 1/13 \approx 0.077$. However, even $\Delta V = 0.2$ typically leads to a spike in the I-cell after a brief delay, so even $g_{EI} = 0.2/(\tau_E V_{rev}) = 0.2/13 \approx 0.015$ will suffice for PING rhythms.

In the CA1 region of the hippocampus, E→E connections are known to have low density (Knowles & Schwartzkroin, 1981). Also, some types

of gamma oscillations are induced by acetylcholine (Fisahn, Pike, Buhl, & Paulsen, 1998), which in turn suppresses recurrent excitatory connections (Hasselmo, 1999). Motivated by these experimental findings and following many previous modeling studies of gamma rhythms (e.g., Whittington, Stanford, Colling, Jefferys, & Traub, 1997), we assume

$$g_{EE} = 0$$

throughout this article. It would be interesting to study the effects of E→E synapses in the presence of noise, particularly in the presence of noisy spiking of the E-cells; however, this will be deferred to future work.

2.5 The Intrinsic Frequency of the I-Cells. The intrinsic frequency ν_I of the I-cells is the frequency at which the I-cells would spike if the E→I synapses were removed. In the presence of I→I synapses, ν_I differs from the frequency of an isolated I-cell and depends on whether the I-cells synchronize.

In many of our arguments, we will make no specific assumption about the neuronal model used for the I-cells, and simply consider ν_I a network parameter. However, we will also apply our general results to the case when the I-cells are modeled as theta neurons. For this, we will need to compute ν_I. The intrinsic frequency ν_I is related to the intrinsic period T_I by $\nu_I = 1000/T_I$. We will discuss how to compute T_I.

2.5.1 Intrinsic Period in the Absence of I→I Synapses. If $g_{II} = 0$, then

$$T_I = \frac{\pi}{\sqrt{I_I}} \tag{2.16}$$

by equation 2.4.

2.5.2 Intrinsic Period in the Presence of I→I Synapses, Assuming Synchronous Network Activity. Assume now that $g_{II} > 0$. We model synapses in the idealized way described by equations 2.13 and 2.14. If the I-cells are in perfect synchrony, the period T_I is the time that it takes for θ to reach π if θ is governed by

$$\begin{aligned} \frac{d\theta}{dt} &= 1 - \cos\theta + \left(I_I - \frac{3}{2} g_{II} e^{-t/\tau_I}\right)(1 + \cos\theta) - g_{II} e^{-t/\tau_I} \sin\theta \ , \\ \theta(0) &= -\pi \ . \end{aligned} \tag{2.17}$$

This cannot be computed analytically, but it is easy to compute numerically.

2.5.3 Intrinsic Period in the Presence of I→I Synapses, Assuming Asynchronous Network Activity. If the I-cells are in complete asynchrony, the function

e^{-t/τ_I} in equation 2.17 is replaced by its time average. (We neglect fluctuations resulting from the finiteness of the network.) Thus, each I-cell is governed by

$$\frac{d\theta}{dt} = 1 - \cos\theta + \left(I_I - \frac{3}{2} g_{II}\bar{s}\right)(1 + \cos\theta) - g_{II}\bar{s}\sin\theta \tag{2.18}$$

with

$$\bar{s} = \frac{1}{T_I}\int_0^{T_I} e^{-t/\tau_I}\, dt = \frac{1 - e^{-T_I/\tau_I}}{T_I/\tau_I}\,. \tag{2.19}$$

If θ obeys equation 2.18, and $\theta(0) = -\pi$, then θ reaches π at time

$$\begin{aligned}
&\int_{-\pi}^{\pi} \frac{d\theta}{1 - \cos\theta + \left(I_I - (3/2)g_{II}\bar{s}\right)(1 + \cos\theta) - g_{II}\bar{s}\sin\theta} \\
&= \left[\frac{\arctan\left(\frac{\tan(\theta/2) - g_{II}\bar{s}/2}{\sqrt{I_I - (3/2)g_{II}\bar{s} - (g_{II}\bar{s})^2/4}}\right)}{\sqrt{I_I - (3/2)g_{II}\bar{s} - (g_{II}\bar{s})^2/4}}\right]_{-\pi}^{\pi} \\
&= \frac{\pi}{\sqrt{I_I - (3/2)g_{II}\bar{s} - (g_{II}\bar{s})^2/4}}.
\end{aligned} \tag{2.20}$$

This formula holds if $I_I - (3/2)g_{II}\bar{s} - (g_{II}\bar{s})^2/4 > 0$. For $I_I - (3/2)g_{II}\bar{s} - (g_{II}\bar{s})^2/4 \le 0$, $\theta = \pi$ is never reached. The period T_I is therefore determined by

$$T_I = \frac{\pi}{\sqrt{I_I - (3/2)g_{II}\bar{s} - (g_{II}\bar{s})^2/4}}\,. \tag{2.21}$$

Note that the right-hand side depends on T_I, since $\bar{s}$ does. We cannot solve this equation analytically. However, it has a unique solution because the right-hand side is a strictly decreasing function of T_I. This solution can easily be found numerically, for instance, using the bisection method.

2.5.4 An Observation on the Effects of I→I Synapses for Weakly Driven I-Cells. A major focus of this letter is the behavior of PING rhythms for weak external drives. We will show later that PING rhythms tend to become noise sensitive when the external drives become weak, but that the noise sensitivity can be counteracted, to some extent, by introducing I→I synapses. This motivates our interest in the effects of I→I synapses in the limit as $I_I \to 0$. The main result of the following discussion is equation 2.23, which will play a role in section 7.

Under the assumption of perfect synchrony of the I-cells, I→I synapses become irrelevant as $I_I \to 0$. In this limit, $T_I \to \infty$, so the decay time τ_I

of the inhibitory synapses becomes negligible in comparison with T_I, and therefore

$$T_I \sim \frac{\pi}{\sqrt{I_I}}$$

as $I_I \to 0$. (The symbol $\sim$ expresses that the ratio of the two quantities converges to 1.)

Under the assumption of complete asynchrony, the I→I synapses remain relevant in the limit as $I_I \to 0$. As $I_I \to 0$, $T_I \to \infty$ and therefore

$$\bar{s} \sim \frac{\tau_I}{T_I} \tag{2.22}$$

by equation 2.19. Using equation 2.22 in equation 2.21, we find that as $I_I \to 0$, the fixed point equation for T_I becomes

$$T_I = \frac{\pi}{\sqrt{I - (3/2)g_{II}\tau_I/T_I - (g_{II}\tau_I/T_I)^2/4}} .$$

This is equivalent to

$$I_I T_I^2 = \frac{3}{2} g_{II}\tau_I T_I + C$$

with

$$C = \pi^2 + \frac{(g_{II}\tau_I)^2}{4} ,$$

so

$$T_I \sim \frac{3}{2}\frac{g_{II}\tau_I}{I_I} + \frac{C}{I_I T_I} \sim \frac{3}{2}\frac{g_{II}\tau_I}{I_I} . \tag{2.23}$$

Comparing equation 2.23 with 2.16, we see that the presence of I→I synapses makes an important difference in the limit as $I_I \to 0$.

2.6 The Asynchronous State. In our simulations, we frequently initialize theta neurons in a state of complete asynchrony. We define here what we mean by "complete asynchrony." Consider a theta neuron with an external drive $I > 0$. Suppose that $\theta(0) = \theta_0 \in (-\pi, \pi)$. The time to the next spike is then

$$\begin{aligned} R = \int_{\theta_0}^{\pi} \frac{dt}{d\theta} d\theta &= \int_{\theta_0}^{\pi} \frac{1}{1 - \cos\theta + I(1 + \cos\theta)} d\theta \\ &= \frac{1}{\sqrt{I}} \left[\arctan \frac{\tan(\theta/2)}{\sqrt{I}} \right]_{\theta_0}^{\pi} \\ &= \frac{1}{\sqrt{I}} \left[\frac{\pi}{2} - \arctan \frac{\tan(\theta_0/2)}{\sqrt{I}} \right] . \end{aligned} \tag{2.24}$$

To initialize a population of uncoupled neurons in complete asynchrony, we choose $R = U\pi/\sqrt{I}$ with $U \in (0,1)$ random, uniformly distributed. We then compute θ_0 from equation 2.24,

$$\theta_0 = 2\arctan\left(\sqrt{I}\tan\left(V\pi/2\right)\right), \tag{2.25}$$

with $V = 1 - 2U$ uniformly distributed in $(-1,1)$.

3 PING in a Simple Two-Cell Network

In this section, we consider a network of a single E-cell and a single I-cell. The E-cell is modeled as a theta neuron; it is assumed to receive external drive $I_E > 0$. We make no explicit assumption about the neuronal model used for the I-cell, but denote by ν_I its intrinsic frequency. (If the I-cell is driven below threshold, $\nu_I = 0$.) We make the following idealizing assumptions:

1. A spike of the E-cell instantaneously triggers a spike of the I-cell but has no effect lasting beyond the spike time.
2. The spike of the I-cell gives inhibitory input to the E-cell in the idealized form described by equation 2.14.
3. The I-cell does not spike again until prompted by the next spike of the E-cell.

Assumptions 1 and 3 imply that the I-cells spike exactly once per oscillation cycle. By strengthening the E→I synapses, one can generate PING-like rhythms in which each I-cell fires multiple times on each oscillation cycle. These rhythms differ from those considered in this letter only in some details of minor interest; for instance, the oscillation frequency is reduced if the I-cell population fires several population spikes on each oscillation cycles. We note that spike doublets of the I-cells play a much subtler and more important role when conduction delays are substantial (Ermentrout & Kopell, 1998). However, in this article, we neglect conduction delays.

If the two cells spike at $t = 0$, the E-cell is governed by the initial value problem

$$\frac{d\theta}{dt} = 1-\cos\theta+\left(I_E-\frac{3}{2}g_{IE}e^{-t/\tau_I}\right)(1+\cos\theta)-g_{IE}e^{-t/\tau_I}\sin\theta \text{ for } t > 0, \tag{3.1}$$

$$\theta(0) = -\pi, \tag{3.2}$$

until it spikes again. We denote by T_P the time at which θ, governed by equations 3.1 and 3.2, reaches π, and write $\nu_P = 1000/T_P$. Assumption 3 then becomes

$$\nu_I \le \nu_P. \tag{3.3}$$

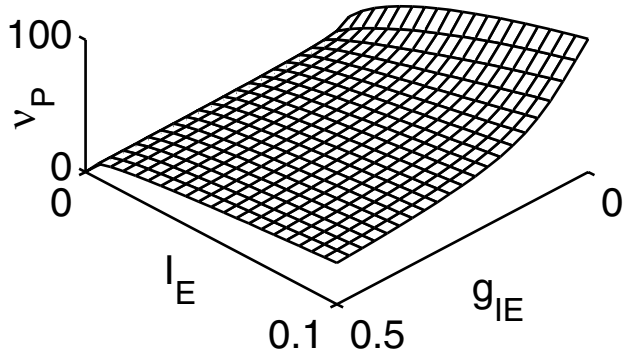

Figure 2: The PING frequency ν_P as a function of g_{IE} and I_E, for $\tau_I = 10$.

We will now discuss the dependence of the frequency ν_P on I_E, g_{IE}, and τ_I. Our main conclusion will be that ν_P depends weakly on I_E and g_{IE} but strongly on τ_I.

For $\tau_I = 10$, Figure 2 shows the graph of ν_P as a function of I_E and g_{IE}. The graph is quite flat in the region in which neither g_{IE}/I_E nor I_E is small. We will argue in later sections that in those regions in which g_{IE}/I_E or I_E are small, PING rhythms are not robust. Specifically, one needs $g_{IE}/I_E > 1$ for rapid and robust synchronization in large networks (see section 5), and PING rhythms with small I_E are highly susceptible to noise in the E-cells (see section 8). Thus, Figure 2 shows that in the most relevant parameter regime, the dependence of ν_P on I_E and g_{IE} is fairly weak.

We will next derive an approximate formula for T_P, valid for sufficiently large g_{IE}/I_E. This formula will confirm that the dependence of T_P on I_E and g_{IE} is weak and also show the importance of τ_I. Defining

$$J = I_E - \frac{3}{2} g_{IE} e^{-t/\tau_I} ,$$

equations 3.1 and 3.2 can be written as follows:

$$\frac{d\theta}{dt} = 1 - \cos\theta + J(1 + \cos\theta) - \frac{2}{3}(I_E - J)\sin\theta \qquad \text{for } t > 0 , \tag{3.4}$$

$$\frac{dJ}{dt} = \frac{I_E - J}{\tau_I} \qquad \text{for } t > 0 , \tag{3.5}$$

$$\theta(0) = -\pi , \tag{3.6}$$

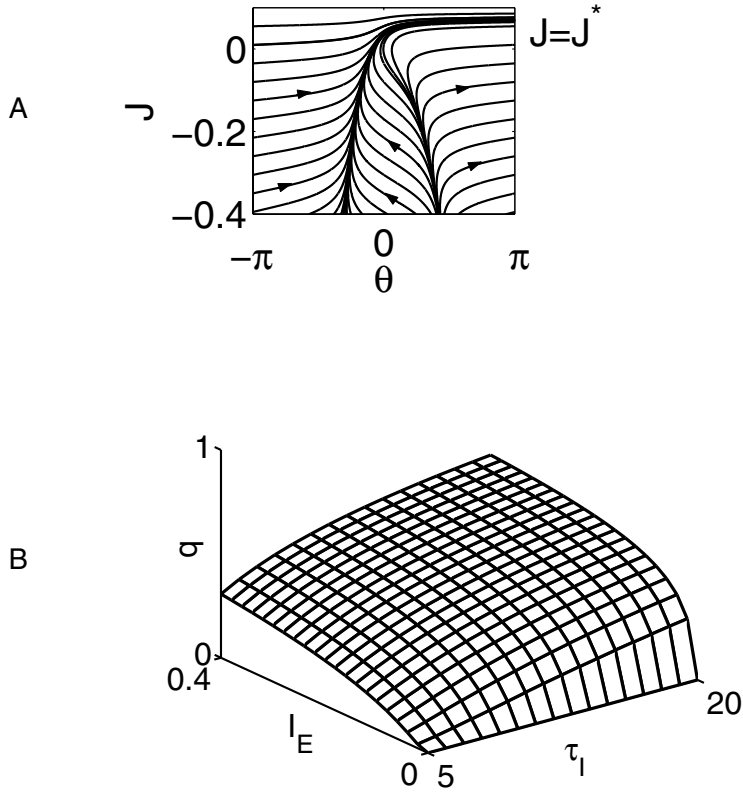

Figure 3: (A) Phase portrait for equations 3.4 and 3.5 with $I_E = 0.1$ and $\tau_I = 10$, with the stable river indicated in bold. (B) $q = (I_E - J^*)/I_E$ as a function of I_E and τ_I.

$$J(0) = I_E - \frac{3}{2} g_{IE} \, . \tag{3.7}$$

We will study the phase portrait for the two-dimensional dynamical system, equations 3.4 and 3.5. This is very similar to a discussion for inhibitory current pulses (not inhibitory synaptic inputs) that we gave earlier (Börgers & Kopell, 2003).

The phase portrait for equations 3.4 and 3.5 is shown in Figure 3A for $I_E = 0.1$ and $\tau_I = 10$. The figure should be extended periodically in θ with period 2π. The flow is upward, in the direction of increasing J. The most striking feature of the phase portrait is the existence of strongly attracting and strongly repelling trajectories. Trajectories of this kind are found in many systems of ordinary differential equations and are called rivers

(Diener, 1985a, 1985b). The figure reveals a stable river, that is, a trajectory,

$$(\theta_s, J_s) \quad \text{with} \quad J_s(t) = I_E - \frac{3}{2} g_{IE} e^{-t/\tau_I}, \tag{3.8}$$

that is attracting in forward time. The stable river is indicated as a bold line in Figure 3A. As $t \to -\infty$, $J_s \to -\infty$, and $\theta_s \to \theta_s^0$, where θ_s^0 is the unique solution in $(-\pi, \pi)$ of

$$1 + \cos\theta + \frac{2}{3}\sin\theta = 0 .$$

(It is easy to see that $\theta_s^0 = -2\arctan(3/2) \approx -1.966$.)

We denote by T^* the time when $\theta_s(T^*) = \pi$, and define

$$J^* = J_s(T^*) \in (0, I_E) . \tag{3.9}$$

We define

$$r = \frac{(3/2)g_{IE}}{I_E} , \tag{3.10}$$

and assume

$$r > 1 , \tag{3.11}$$

so $J(0) < 0$. If $J(0)$ is sufficiently negative, the trajectory $(\theta(t), J(t))$ is rapidly attracted to $(\theta_s(t), J_s(t))$. At the time when $\theta = \pi$, we therefore have $J \approx J^*$, or $t \approx T^*$. Thus, T_P is approximately T^*.

Equations 3.8 and 3.9 imply that

$$T^* = \ln\left(\frac{(3/2)g_{IE}}{I_E - J^*}\right)\tau_I . \tag{3.12}$$

We write

$$q = q(\tau_I, I_E) = \frac{I_E - J^*}{I_E} \in (0, 1) . \tag{3.13}$$

Figure 3B shows the graph of q. From equations 3.10, 3.12, and 3.13,

$$T^* = \ln\left(\frac{r}{q}\right)\tau_I . \tag{3.14}$$

Of course, this is not an explicit formula for T^*, since q depends on I_E and τ_I and is not given by an explicit formula. Equation 3.14 does, however,

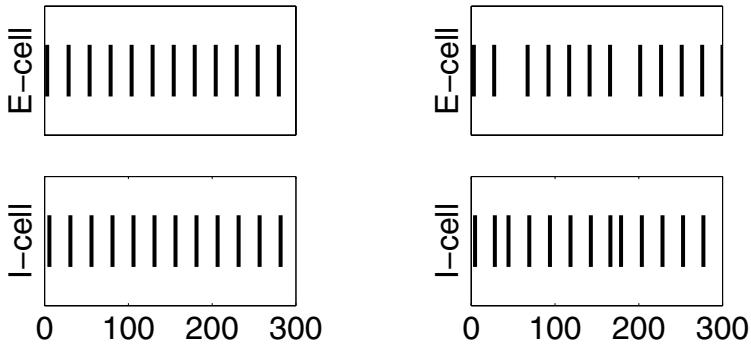

Figure 4: From PING (left panel) to phase walkthrough (right panel) as a result of raising drive to the I-cell.

explicitly describe the dependence of T^* on g_{IE}, since the only quantity on the right-hand side of equation 3.14 depending on g_{IE} is $r = (3/2)g_{IE}/I_E$.

We have concluded

$$T_P \approx \ln\left(\frac{r}{q}\right)\tau_I\,, \tag{3.15}$$

if r is sufficiently large. Numerical experiments show that $r = 3$ is sufficient for this formula to be quite accurate. Figure 3B shows that the graph of q is fairly flat unless I_E is small. In a parameter regime in which q is approximately constant, formula 3.15 shows that T_P depends strongly (namely, approximately linearly) on τ_I, but only weakly (namely, logarithmically) on g_{IE} and I_E.

4 The Phase Walkthrough Boundary

A necessary condition for the PING mechanism to work is that the I-cells spike only when prompted by the E-cells, not independently. This is trivially true if the drive to the I-cells is subthreshold, that is, $\nu_I = 0$. If $\nu_I > 0$, then the PING mechanism works only if the frequency of the rhythm is greater than the intrinsic frequency of the I-cells. Figure 4 illustrates, using a network of a single E-cell and a single I-cell, what happens when this condition is not met. (The figure indicates spike times.) We refer to the phenomenon shown in Figure 4 as phase walkthrough of the I-cells.

Figure 5 shows, in various different ways, that phase walkthrough occurs more easily when I_E is smaller or g_{IE} is larger, in other words, when the PING frequency is lower. The figure also shows that I→I synapses protect against phase walkthrough. We will now discuss the details of Figure 5.

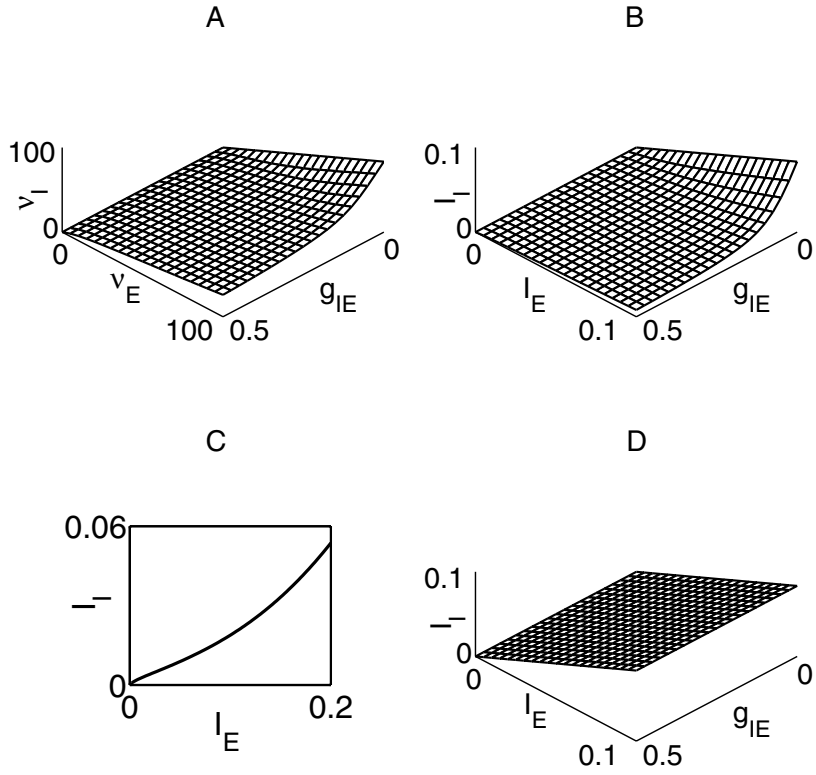

Figure 5: Phase walkthrough boundary for $\tau_I = 10$ (A) in (g_{IE}, ν_E, ν_I)-space, (B) in (g_{IE}, I_E, I_I)-space for $g_{II} = 0$, (C) in the (I_E, I_I)-plane, for $g_{II} = 0$ and $g_{IE} = 0.2$, (D) in (g_{IE}, I_E, I_I)-space, for $g_{II} = g_{IE}$.

4.1 The Phase Walkthrough Condition. In the simple two-cell network of section 3, a necessary and sufficient condition for phase walkthrough of the I-cells to be avoided is

$$\nu_I \leq \nu_P \, . \tag{4.1}$$

The equation

$$\nu_I = \nu_P \tag{4.2}$$

(or equivalently $T_I = T_P$) defines a hypersurface in parameter space that we call the phase walkthrough boundary. As discussed in section 3, ν_P is a function of I_E, g_{IE}, and τ_I. Since $\nu_E = (1000/\pi)\sqrt{I_E}$, we can also think of ν_P as a function of ν_E, g_{IE}, and τ_I. For given ν_E, g_{IE}, and τ_I, it is easy to

calculate ν_P numerically with great (ten-digit) accuracy. We first determine the time T_p at which θ, governed by equations 3.1 and 3.2, reaches π, and then compute $\nu_P = 1000/T_p$. For $\tau_I = 10$, Figure 5A shows the phase walkthrough boundary in (g_{IE}, ν_E, ν_I)-space. If (g_{IE}, ν_E, ν_I) lies below the surface in Figure 5A, a PING rhythm is possible. Above the surface, there is no PING rhythm because of phase walkthrough.

Note that slowing the rhythm without reducing drive to the I-cell eventually results in $\nu_I > \nu_P$, that is, in phase walkthrough.

4.2 I→I Synapses Protect Against Phase Walkthrough. Since ν_I is a decreasing function of g_{II}, I→I synapses make phase walkthrough of the I-cells less likely to occur. (Recall that by the notational conventions of section 2, the definition of ν_I takes I→I synapses into account, but ν_E denotes the frequency of the E-cells in the absence of any synapses.) To make this quantitative, we must assume a specific model for the I-cell. For the remainder of this section, we therefore assume that the I-cell is a theta neuron. We still make assumptions 1 and 2 of section 3, and we also assume that I→I synapses take the idealized form given by equation 2.14.

For fixed values of τ_I and g_{II}, the phase walkthrough boundary can then be thought of as a surface in (g_{IE}, I_E, I_I)-space. For $\tau_I = 10$ and $g_{II} = 0$, this surface is plotted in Figure 5B. The surface in Figure 5B is thus identical to that of Figure 5A, except for the choice of coordinates. The parameter ν_I in Figure 5A is replaced by I_I in Figure 5B. Equation 2.16 yields the relation between ν_I and I_I. (Note that $\nu_I = 1000/T_I$.) Figure 5B shows that in the parameter regimes of interest to us ($r > 1$, that is, $g_{IE} > (2/3)I_E$)), I_I must be much smaller than I_E for PING to be possible.

In Figure 5C, we show a section through the surface of Figure 5B. In addition to fixing $\tau_I = 10$ and $g_{II} = 0$ as in Figure 5B, $g_{IE} = 0.2$ is fixed as well. The curve in Figure 5C is the graph of a function of I_E. For later reference, we denote this function by $F = F(I_E)$, suppressing in the notation the dependence on τ_I, g_{II}, and g_{IE}. Thus, the curve shown in Figure 5C is given by

$$I_I = F(I_E)\ . \tag{4.3}$$

Phase walkthrough occurs above the curve, but not below it.

The surface in Figure 5B changes dramatically when g_{II} is taken to be equal to g_{IE}. It is easy to see that in this case, the walkthrough boundary is given by

$$I_I = I_E \tag{4.4}$$

(see Figure 5D). Thus, I→I synapses have a stabilizing effect, greatly enlarging the parameter regime in which PING is possible.

5 PING in Networks of More Than Two Cells

The key to PING rhythms in networks of more than two cells lies in the fact that a population of uncoupled neurons receiving a single common strong inhibitory input pulse synchronizes. In this section, we give an explanation of this synchronization mechanism and illustrate it with numerical examples. The main conclusion of this section is that rapid and robust synchronization in large networks requires $r = (3/2)g_{IE}/I_E > 1$.

In earlier work (Börgers & Kopell, 2003), we discussed the synchronization of a population of theta neurons by an inhibitory current pulse. We present here a very similar discussion referring to an inhibitory synaptic pulse.

A single theta neuron receiving an inhibitory synaptic input at $t = 0$ is described by equations 3.4 and 3.5, with initial conditions $\theta(0) = \theta_0$, and equation 3.7. Synchronization of a population of uncoupled theta neurons by a single inhibitory synaptic pulse can be understood from the phase portrait in Figure 3A. Recall that the trajectory (θ_s, J_s) indicated as a bold line in Figure 3A, the "stable river," attracts nearby trajectories. Also recall that T^* is defined by $\theta_s(T^*) = \pi$ and J^* by $J^* = J_s(T^*)$.

Assume, as in section 3, $r > 1$, so $J(0) < 0$. If $J(0)$ is sufficiently negative and θ_0 is sufficiently far from π, $(\theta(t), J(t))$ is rapidly attracted to the stable river. At the time when $\theta = \pi$, we therefore have $J \approx J^*$, or $t \approx T^*$. Thus, the first spike after time zero occurs approximately at time T^*.

If θ_0 is close to π, then $\theta(t)$ quickly passes through π and is then rapidly attracted to $(\theta_s(t) + 2\pi, J_s(t))$. (Recall that Figure 3A should be thought of as extended periodically in θ with period 2π.) When $\theta(t)$ reaches 3π, then $J \approx J^*$ and therefore $t \approx T^*$. Thus, in that case, a spike occurs soon after time zero, followed by a spike approximately at time T^*.

Only for values of θ_0 in a narrow transition band is $(\theta(t), J(t))$ attracted to neither $(\theta_s(t), J_s(t))$ nor $(\theta_s(t) + 2\pi, J_s(t))$. A population of E-cells is approximately synchronized by an inhibitory pulse with sufficiently large r because T^* is independent of θ_0.

Figure 6A shows a simulation for a network as described in section 2,

$$g_{EI} = 0.05, \quad g_{IE} = 0.20, \quad g_{II} = 0, \quad I_E = 0.1 \quad (\nu_E \approx 101), \quad I_I = 0.002.$$

(Other parameter values are as specified in section 2.) The common inhibitory input received by all E-cells leads to their rapid synchronization as a result of the mechanism described earlier. This in turn leads to synchronization of the I-cells, which are driven by the E-cells. Note that here,

$$r = \frac{(3/2)g_{IE}}{I_E} = \frac{0.3}{0.1} = 3\,.$$

PING rhythms are possible even for $r < 1$. For instance, Figure 6B shows results similar to those of Figure 6A, but with $g_{IE} = 0.05$, corresponding to $r = 0.75$. A rhythm appears, but only after a number of periods, not

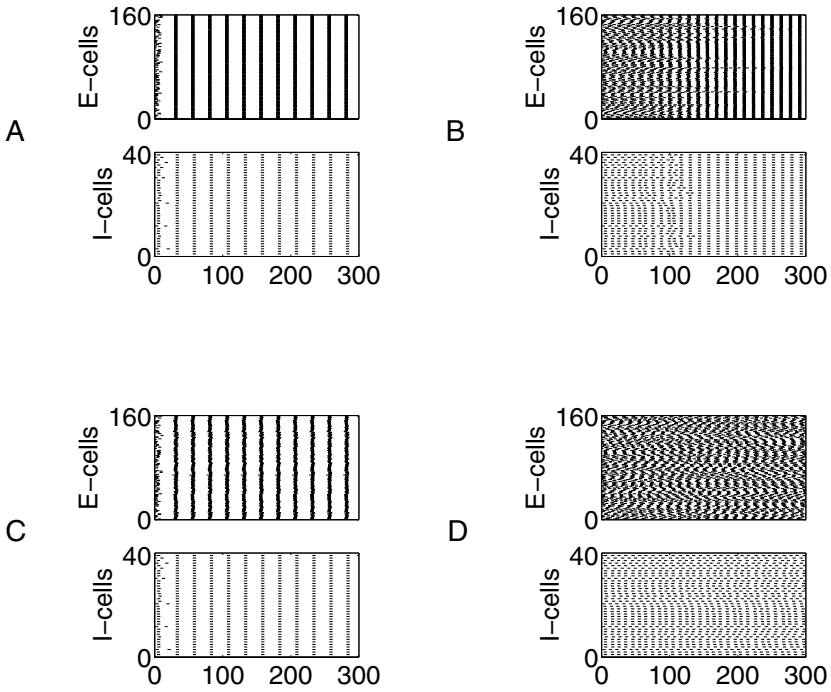

Figure 6: (A) PING with strong inhibitory synapses ($g_{EI} = 0.05$, $g_{IE} = 0.2$, $g_{II} = 0, I_E = 0.1, I_I = 0.002$). (B) PING with weak inhibitory synapses ($g_{IE} = 0.05$; all other parameter values as in A). (C) As in A, with 5% heterogeneity in I_E. (D) As in B, with 5% heterogeneity in I_E.

immediately. Thus, when $r \leq 1$, PING may still be possible, but it is less attracting and more difficult to analyze. Numerical experiments suggest that PING with $r \leq 1$ is also highly sensitive to heterogeneity. As an example, we introduce 5% heterogeneity in I_E. That is, we take I_E to be a normally distributed random number with mean 0.1 and standard deviation 0.005. Figure 6A turns into Figure 6C—the rhythm is barely affected. However, Figure 6B turns into Figure 6D—the rhythm is destroyed. The effect of heterogeneity in I_E is to spread out the spiking of the E-cells. If r is sufficiently large, each population spike of the I-cells approximately erases the memory of the past, bringing the E-cells back together and preventing the effects of heterogeneity from accumulating over time. In our numerical experience, at least $r \approx 3$ is required if the rhythm is to survive heterogeneity in network parameter values on the order of 20%.

6 The Suppression Boundary

As seen in section 4, in a two-cell network (or, equivalently, in a larger network in which the E-cells and the I-cells are perfectly synchronized), PING is possible only if the intrinsic frequency ν_I of the I-cells is sufficiently small. If the I-cells intrinsically spike too rapidly, phase walkthrough occurs.

In a network with many cells, there is another way in which rapid spiking of the I-cells can destroy PING: the I-cells can suppress the E-cells altogether. The I-cells are most effective at suppressing the E-cell when they are asynchronous. For linear integrate-and-fire neurons, this is proved in appendix A. Although we have not proved it for theta neurons, numerical evidence suggests that it is true in that case as well. We therefore assume in this section that the I-cells spike in complete asynchrony and ask under which circumstances the I-cells suppress the E-cells.

Figure 7 shows, in various different ways, that suppression of the E-cells occurs more easily when I_E is smaller or g_{IE} is larger, in other words, when the PING frequency is lower. In this section, we will discuss the four panels of Figure 7 in detail. We will show that the quantity determining how easily suppression of the E-cells occurs is the ratio g_{IE}/I_E, which, up to the constant factor 3/2, is r.

6.1 The Suppression Condition. Consider a large population of I-cells, spiking in asynchrony, acting on a single E-cell driven above threshold. We ask under which conditions spiking in the E-cell will be prevented altogether by the inhibition. We model the synaptic gating variable in the idealized way described by equation 2.14. Because the I-cells are assumed to spike in asynchrony, the term $s(t)$ in equation 2.13 is replaced by its time average. (We neglect fluctuations resulting from the finiteness of the network.) Thus, the equation governing the target neuron is

$$\frac{d\theta}{dt} = 1 - \cos\theta + \left(I_E - \frac{3}{2} g_{IE}\bar{s}\right)(1 + \cos\theta) - g_{IE}\bar{s}\sin\theta, \tag{6.1}$$

with $\bar{s}$ defined in equation 2.19. The E-cell escapes suppression if and only if

$$\frac{3}{2} g_{IE}\bar{s} + \frac{1}{4}\left(g_{IE}\bar{s}\right)^2 < I_E\ . \tag{6.2}$$

To see this, replace g_{II} by g_{IE} and I_I by I_E in equation 2.20. Since we assume $I_E \ll 1$, this is approximately equivalent to

$$\frac{3}{2} g_{IE}\bar{s} < I_E\ .$$

Using the definition of r, equation 3.10, this condition becomes

$$\bar{s} < \frac{1}{r}\ . \tag{6.3}$$

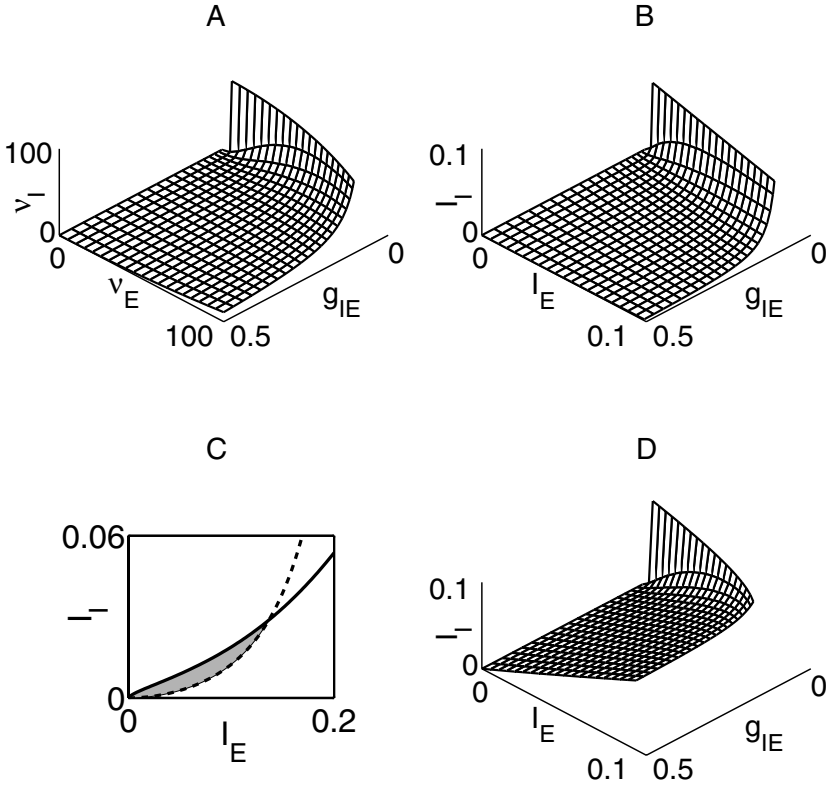

Figure 7: Suppression boundary for $\tau_I = 10$, (A) in (g_{IE}, ν_E, ν_I)-space, (B) in (g_{IE}, I_E, I_I)-space, for $g_{II} = 0$, (C) in the (I_E, I_I)-plane for $g_{II} = 0$ and $g_{IE} = 0.2$ (dashes), together with the phase walkthrough boundary (solid) and the region of bistability (shaded), (D) in (g_{IE}, I_E, I_I)-space, for $g_{II} = g_{IE}$.

The equation

$$\overline{s} = \frac{1}{r} \tag{6.4}$$

defines a hypersurface in parameter space that we call the suppression boundary. Since $\overline{s}$ depends on only $T_I/\tau_I = 1000/(\nu_I\tau_I)$ (see equation 2.19), the suppression boundary could be drawn as a surface in $(g_{IE}, \nu_E, \nu_I\tau_I)$-space. However, for easier comparison with Figure 5A, we set $\tau_I = 10$ and plot, in Figure 7A, the suppression boundary as a surface in (g_{IE}, ν_E, ν_I)-space. If (g_{IE}, ν_E, ν_I) lies below the surface in Figure 7A, suppression of the E-cells by asynchronous activity of the I-cells is impossible. Above the surface, suppression occurs if the I-cells spike asynchronously.

Asynchronous activity of the I-cells can simply be the result of initial conditions, in the absence of any mechanism synchronizing the I-cells. (The E-cells cannot synchronize the I-cells if they are suppressed.) It can also be the result of stochastic external inputs to the I-cells. In that case, each I-cell spikes in an irregular fashion. However, if T_I is taken to be the average interspike interval, then equation 6.3 is still the condition under which the E-cells escape suppression. This will be discussed further in section 9.

Figure 7A shows that in a large portion of parameter space (the portion where the surface is flat), PING rhythms are highly susceptible to suppression of the E-cells as a result of asynchronous activity of the I-cells. (Recall that suppression occurs above the surface shown in Figure 7A.) In this portion of parameter space, PING rhythms are easily abolished by noisy external drive to the I-cells (see section 9). Equation 6.3 shows that r is the quantity that matters here: the larger r, the more severe is condition 6.3.

6.2 Slow PING Rhythms Are Typically Susceptible to Suppression of the E-Cells. If a PING rhythm is slowed by lowering ν_E, that is, lowering I_E, with all other parameter values fixed, then r grows, and therefore the rhythm becomes more susceptible to suppression of the E-cells by the I-cells. Similarly, if a PING rhythm is slowed by raising g_{IE}, with all other parameter values fixed, then r grows, and the rhythm again becomes increasingly susceptible to suppression of the E-cells.

6.3 Suppression of the E-cells Can Be Avoided Even at Low Frequencies by Careful Parameter Tuning. Slow PING rhythms are not impossible. If $I_E \to 0$ and $g_{IE} \to 0$ in such a way that r remains fixed, then $\nu_P \to 0$. This can be seen from Figure 2 or from equation 3.15 in conjunction with Figure 3B (which shows that q decreases as I_E decreases and $q \to 0$ as $I_E \to 0$). However, the right-hand side of equation 6.3 remains unchanged in this limit. Thus, a PING rhythm with small I_E and proportionally small g_{IE} is slow, but not susceptible to suppression of the E-cells by the I-cells.

6.4 I→I Synapses Protect Against Suppression. I→I synapses make it harder for the I-cells to suppress the E-cells for two reasons. First, they often destabilize asynchrony of the I-cells. However, even if the I-cells were to remain completely asynchronous, I→I synapses would make it harder for the I-cells to suppress the E-cells, by lowering ν_I.

To illustrate the latter point, we now assume that the I-cells are theta neurons. As before, we assume that I→I synapses take the idealized form given by equation 2.14. For fixed τ_I and g_{II}, we draw the suppression boundary as a surface in (g_{IE}, I_E, I_I)-space. For $\tau_I = 10$ and $g_{II} = 0$, this is shown in Figure 7B. The dashed curve in Figure 7C shows a section through the surface of Figure 7B. In addition to fixing $\tau_I = 10$, $g_{II} = 0$, $g_{IE} = 0.2$ is fixed as well. This curve is the graph of a function of I_E. For later reference, we denote this function by $G = G(I_E)$, suppressing in the notation the dependence on

τ_I, g_{IE}, and g_{II}. Thus, the dashed curve in Figure 7C is given by

$$I_I = G(I_E) \, . \tag{6.5}$$

The phase walkthrough boundary for the same parameter values was plotted in Figure 5C; for comparison, it is reproduced in Figure 7C (solid curve).

The two curves in Figure 7C intersect each other, enclosing a region, shaded in Figure 7C, that lies above the suppression boundary (so suppression of the E-cells by asynchronous activity of the I-cells is possible), but below the phase walkthrough boundary (so PING is possible as well). This is a region of bistability; it will be discussed further in section 7.

Figure 7B changes dramatically when g_{II} is taken to be equal to g_{IE} (see Figure 7D). The region in phase space in which suppression of the E-cells by the I-cells is impossible (the region below the surface) is greatly enlarged by the I→I synapses. As will be shown in the next section, there is no region of bistability in this case.

7 A Region of Bistability

We observed in section 6 that Figure 7C shows a region of bistability in parameter space, a region in which both asynchronous activity of the I-cells with suppression of the E-cells and PING are possible. Which of these two states occurs depends on initial conditions. This observation is not centrally important here, but it is an interesting example demonstrating that PING rhythms can be locally but not globally attracting network states.

In this section, we give analytic arguments demonstrating the existence of the region of bistability (or, to be more precise, demonstrating that the two curves in Figure 7C must intersect in a point other than the origin). We also give a numerical example illustrating the bistability.

The solid curve in Figure 7C, the phase walkthrough boundary, is the graph of a function. Recall from section 4 that we denote this function by F, so the curve in Figure 7C is given by $I_I = F(I_E)$. We shall first show

$$F'(0) = 1 \tag{7.1}$$

and

$$\lim_{I_E \to \infty} F(I_E) = \infty \, . \tag{7.2}$$

To prove equation 7.1, note that $T_P \to \infty$ as $I_E \to 0$. Thus, the (fixed) decay time τ_I becomes negligible in comparison with T_P. This implies that the inhibitory synapses become negligible, so $T_P \sim T_E = \pi/\sqrt{I_E}$, and $T_I \sim \pi/\sqrt{I_I}$. The phase walkthrough boundary is generally given by $T_P = T_I$. In the limit as $I_E \to 0$, this means $\pi/\sqrt{I_E} \sim \pi/\sqrt{I_I}$, or $I_E \sim I_I$, that is, equation 7.1.

Figures 5B and 5C appear to suggest that $F'(0)$ is positive, but much smaller than 1, in contradiction to the result just derived. The explanation is that I_E has to be extremely close to 0 for $F'(I_E)$ to come close to 1. A numerically computed blow-up of Figure 5C near the origin indeed confirms that $F'(0) = 1$.

To prove equation 7.2, we first note that F increases as g_{II} increases: the greater g_{II}, the more drive I_I to the I-cells is needed for phase walkthrough to occur. Therefore, equation 7.2 follows for $g_{II} > 0$ if it can be shown for $g_{II} = 0$. To prove equation 7.2 for $g_{II} = 0$, we note that in the limit $I_E \to \infty$, the I→E synapses become negligible as well, but for a different reason: the terms, including the factor I_E in the equation of the E-cell, dominate all others, in particular, the terms modeling the synapse. As a result, $T_P \sim T_E$ as $I_E \to \infty$. The phase walkthrough boundary is generally given by $T_P = T_I$. In the limit as $I_E \to \infty$, this means $T_E \sim T_I$. For $g_{II} = 0$, this means $\pi/\sqrt{I_E} \sim \pi/\sqrt{I_I}$, or $I_E \sim I_I$. This implies equation 7.2.

The dashed curve in Figure 7C, the suppression boundary, is the graph of a function as well. Recall from section 6 that we denote this function by G, so the dashed curve in Figure 7C is given by $I_I = G(I_E)$. We next show

$$G'(0) = \frac{g_{II}}{g_{IE}} \tag{7.3}$$

and

$$\lim_{I_E \to (3/2)g_{IE}} G(I_E) = \infty \,. \tag{7.4}$$

To show equation 7.3, note that as $I_E \to 0$, $I_I = G(I_E) \to 0$; therefore, $T_I \to \infty$, and

$$\bar{s} \sim \frac{\tau_I}{T_I}$$

by equation 2.19. Thus, the suppression boundary becomes

$$\frac{T_I}{\tau_I} \sim r \tag{7.5}$$

by equation 6.4. Assuming $g_{II} > 0$, using equation 2.23, this becomes

$$\frac{(3/2)g_{II}}{I_I} \sim \frac{(3/2)g_{IE}}{I_E},$$

or

$$I_I \sim \frac{g_{II}}{g_{IE}} I_E,$$

that is, equation 7.3. If $g_{II} = 0$, we use equation 2.16 to turn equation 7.5 into

$$\frac{\pi}{\sqrt{I_I}} \sim \frac{(3/2)g_{IE}}{I_E}$$

or

$$I_I \sim \pi^2 \frac{I_E^2}{(9/4)g_{IE}^2}.$$

Thus, equation 7.3 holds for $g_{II} = 0$ as well.

As $I_E \to (3/2)g_{IE}$, $r \to 1$. The suppression boundary is given by

$$\frac{1 - e^{-T_I/\tau_I}}{T_I/\tau_I} = \frac{1}{r} \tag{7.6}$$

(see equations 6.4 and 2.19). The left-hand side of equation 7.6 can easily be shown to be a strictly decreasing function of T_I/τ_I that tends to 1 as $T_I/\tau_I \to 0$. Thus, as $r \to 1$, $T_I/\tau_I \to 0$, so $I_I \to \infty$. This proves equation 7.4.

Equations 7.1 to 7.4, taken together, imply that the suppression and phase walkthrough boundaries in the (I_E, I_I)-plane must intersect (in a point other than the origin) as long as $g_{II} < g_{IE}$.

We present a numerical example illustrating the bistability that our theoretical arguments predict. We use

$$g_{IE} = 0.2, \quad g_{EI} = 0.05, \quad g_{II} = 0$$

and

$$(I_I, I_E) = (0.0025, 0.03)\ ,$$

a point inside the region of bistability. We initialize the I-cells asynchronously (see section 2.6). If we initialize all E-cells at $\theta = -\pi/2$, complete suppression of the E-cells results, as shown in Figure 8A. On the other hand, if we initialize the E-cells at $\theta = \pi/2$, they start out so close to spiking that they are able to spike before enough inhibition has built up to suppress them. This moves the I-cells away from asynchrony, removing their ability to suppress the E-cells. The result is the PING rhythm shown in Figure 8B. The two simulations producing the two panels of Figure 8 are identical, except for initial conditions.

8 Phase Walkthrough of the I-Cells Resulting from Stochastic Spiking of the E-Cells

In this section, we consider the effects of noisy spiking of the E-cells, for instance, as a result of stochastic external input. We show that noisy spiking of the E-cells disrupts PING rhythms by causing phase walkthrough of the I-cells. We give an approximate analysis of the conditions under which noise in the E-cells results in phase walkthrough of the I-cells. Our analysis is not very accurate quantitatively (we will explain why); however, it does reveal that slower PING rhythms are much more vulnerable to noise in the E-cells than faster ones.

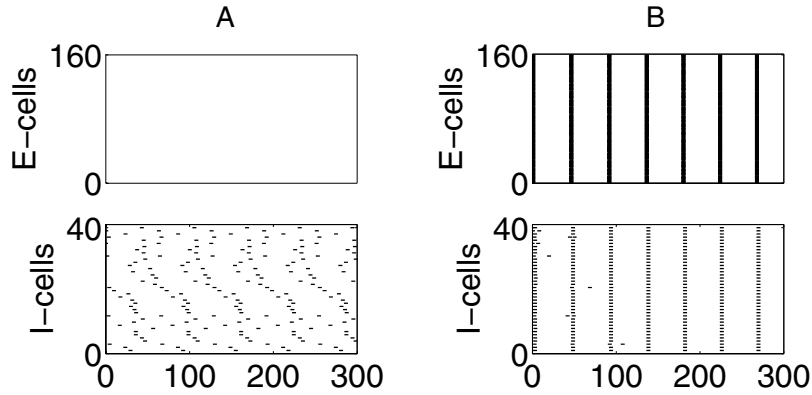

Figure 8: Example illustrating bistability. Suppression of the E-cells (A) or a rhythm (B) are possible with the same parameter values ($g_{EI} = 0.05$, $g_{IE} = 0.2$, $g_{II} = 0$, $I_E = 0.03$, $I_I = 0.0025$), different initial conditions.

In our simulations, we introduce random spiking of the E-cells as follows. At randomly selected times,

$$t_{i1} < t_{i2} < \ldots , \quad 1 \le i \le N_E ,$$

the ith E-cell is forced to spike; that is, the value of θ associated with it is instantaneously reset to $-\pi$, and the synaptic gating variable s associated with it is set to 1. We assume that the time intervals between forced spikes,

$$t_{i,k+1} - t_{i,k} , \quad 1 \le i \le N_E , \quad k = 1, 2, ...,$$

are independent of each other and exponentially distributed, with a common expected value T_{SE}. (The subscript S stands for "stochastic.") We define

$$\nu_{SE} = \frac{1000}{T_{SE}} . \tag{8.1}$$

This is the average frequency of the random spiking of the E-cells.

Figures 9C, 9D, and 9F (discussed in detail shortly) show examples of rhythms that persist in spite of random spiking in the E-cells. When an E-cell spikes out of order, it is temporarily out of synchrony with the bulk of the E-cells. It may or may not participate in the next population spike of the E-cells. However, it is brought back into synchrony with the bulk of the E-cells by the next population spike of the I-cells.

If a large fraction of the E-cells spikes out of order, the number of E-cells participating in the population spikes may be reduced significantly. The population spikes of the E-cells may then no longer suffice to trigger population spikes of the I-cells. This effect is neglected in the analysis given

below, as is justified if g_{EI} is sufficiently large and/or if the ratio ν_{SE}/ν_P is sufficiently small. For example, in Figure 9D, a large fraction of all E-cells spike out of order, but g_{EI} is so large that those E-cells that participate in the population spikes still suffice to prompt the I-cells.

8.1 Analysis. The low-frequency random spiking of some of the E-cells between population spikes generates extra excitatory drive to the I-cells. If each I-cell receives input from sufficiently many E-cells, this drive is nearly constant. For two special cases, we will now analyze when the extra drive to the I-cells results in phase walkthrough.

We assume here that the I-cells are modeled as theta neurons. However, we find it convenient to use the dependent variable V instead of θ (see section 2.1). In the absence of synaptic input, the equation of an I-cell is then

$$\frac{dV}{dt} = 2V(V-1) + Q_I$$

(see equation 2.7). The relation between Q_I and I_I is

$$I_I = 2Q_I - 1$$

(see equation 2.10).

The random spiking of the E-cells approximately adds the term

$$Q_{SI} = g_{EI}\frac{1}{T_{SE}}\int_0^{T_{SE}} e^{-t/\tau_E}dtV_{rev} = g_{EI}\frac{1-e^{-T_{SE}/\tau_E}}{T_{SE}/\tau_E}V_{rev} \tag{8.2}$$

to Q_I (compare equation 2.12). The average of e^{-t/τ_E} over $[0, T_{SE}]$ appears in this formula because the stochastic spiking of the E-cells is assumed to be asynchronous. We have also used the approximation $V_{rev} - V \approx V_{rev}$ in equation 8.2; this is reasonable because V is near 0 except during spikes. We are interested in low-frequency random spiking in the E-cells, so $T_{SE} \gg \tau_E = 2$, and therefore the term e^{-T_{SE}/τ_E} in equation 8.2 is negligible:

$$Q_{SI} \approx \frac{g_{EI}\tau_E V_{rev}}{T_{SE}}\,. \tag{8.3}$$

Q_{SI} is added to Q_I, so $I_I = 2Q_I - 1$ turns into $I_I + 2Q_{SI}$. Denoting by $f_I(I)$ the frequency of an I-cell receiving drive I, the condition under which phase walkthrough of the I-cells is avoided becomes approximately

$$f_I\left(I_I + \frac{2g_{EI}\tau_E V_{rev}}{T_{SE}}\right) \le \nu_P \tag{8.4}$$

(see equation 4.1). If $g_{II} = 0$, then $f_I(I) = (1000/\pi)\sqrt{I}$ by equations 2.3 and 2.5. Therefore, inequality 8.4 becomes

$$\frac{1000}{\pi}\sqrt{I_I + \frac{2g_{EI}\tau_E V_{rev}}{T_{SE}}} \le \nu_P$$

or, equivalently,

$$\frac{\nu_{SE}}{1000} \leq \frac{\pi^2(\nu_P/1000)^2 - I_I}{2g_{EI}\tau_E V_{rev}} \,. \tag{8.5}$$

Inequality 8.5 was derived assuming $g_{II} = 0$. For $g_{II} > 0$, the rhythm can withstand more drive to the I-cells, and therefore more random spiking of the E-cells. In the special case $g_{II} = g_{IE}$, the condition under which phase walkthrough of the I-cells is avoided is

$$I_I + 2Q_{SI} \leq I_E \tag{8.6}$$

(compare equation 4.4). With the approximation 8.3, inequality 8.6 is equivalent to

$$\frac{\nu_{SE}}{1000} \leq \frac{I_E - I_I}{2g_{EI}\tau_E V_{rev}} \,. \tag{8.7}$$

To highlight the similarity between this inequality and equation 8.5, we note that

$$I_E = \pi^2(\nu_E/1000)^2$$

by equations 2.3 and 2.5, so inequality 8.7 can be written as

$$\frac{\nu_{SE}}{1000} \leq \frac{\pi^2(\nu_E/1000)^2 - I_I}{2g_{EI}\tau_E V_{rev}} \,. \tag{8.8}$$

Note that equation 8.8 is obtained from equation 8.5 if ν_P is replaced by ν_E. Both formulas show that slower rhythms (smaller ν_P or smaller ν_E) are more vulnerable to noisy activity in the E-cells than faster ones.

8.2 Numerical Examples.

8.2.1 Too Much Noise in the E-Cells Leads to Phase Walkthrough of the I-Cells. Figure 9A shows results of a simulation with

$$g_{EI} = 0.05, \;\; g_{IE} = 0.20, \;\; g_{II} = 0, \;\; I_E = 0.1 \;\; (\nu_E \approx 101), \;\; I_I = 0 \,. \tag{8.9}$$

(Other parameter values are as specified in section 2.) A rhythm at frequency $\nu_P \approx 40$ is seen. We remark that $r = (3/2)g_{IE}/I_E = 3$ here. Inserting the parameter values 8.9 in inequality 8.5, we find that the rhythm should hold up for $\nu_{SE} \leq 12.15$. This prediction is not very accurate. With $\nu_{SE} = 7$, phase walkthrough occurs already, as shown in Figure 9B. (Note that Figure 9B is indeed a noisy analog of the sort of phase walkthrough depicted in Figure 4.) Thus, the breakdown occurs earlier in our simulation than predicted

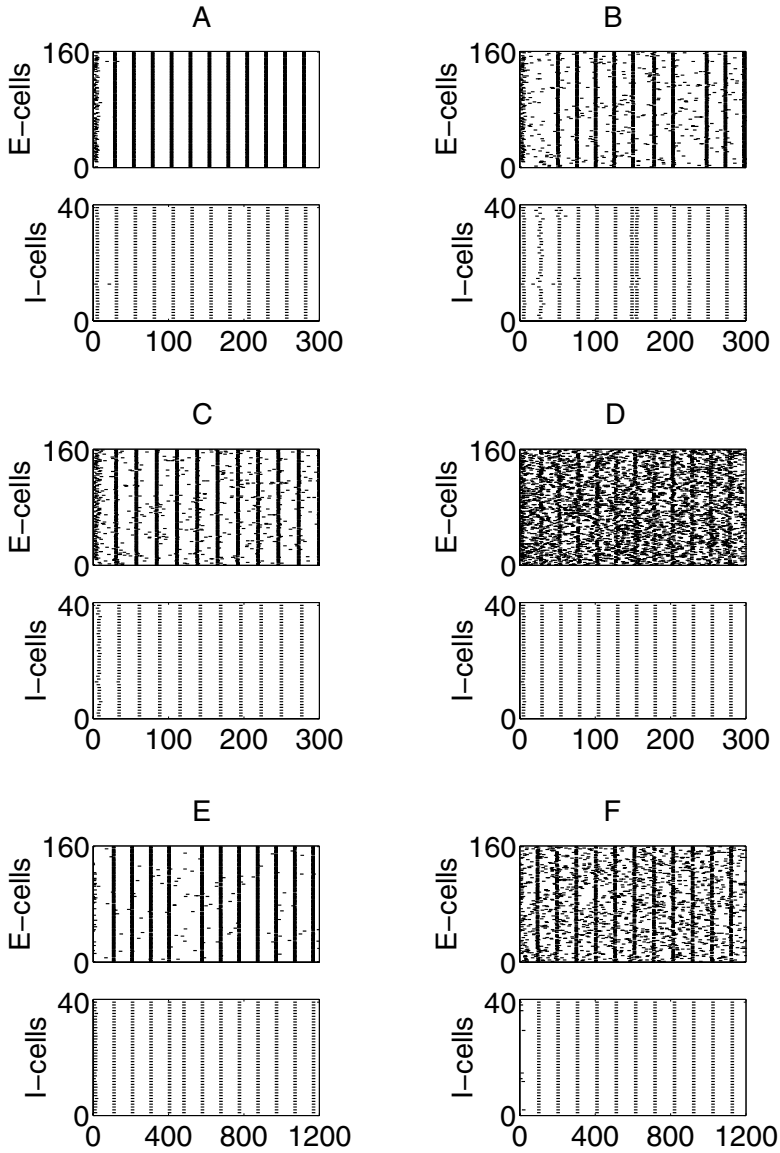

Figure 9: (A) Gamma frequency PING rhythm ($g_{EI} = 0.05$, $g_{IE} = 0.2$, $g_{II} = 0$, $I_E = 0.1$, $I_I = 0$). (B) Low-frequency stochastic spiking in the E-cells leads to phase walkthrough in the I-cells. (C) Phase walkthrough is counteracted by reducing g_{EI} 0.02. (D) I→I synapses ($g_{II} = g_{IE}$) make the rhythm astonishingly robust to noise in the E-cells. (E) A slow PING rhythm ($I_E = 0.003$; all other parameter values as in *A*) is highly sensitive to noise in the E-cells. (F) Noise sensitivity can be greatly reduced, even for the slow rhythm, by setting $g_{II} = g_{IE}$ and reducing g_{EI} to 0.01.

by our theory. To understand this discrepancy, we took a detailed look at the simulation underlying Figure 9B, focusing on the three population spikes of the I-cells that occur out of order, not prompted by the E-cells, in Figure 9B. Immediately before each of these population spikes, the actual drive to the I-cells rises significantly above that predicted by formula 8.2, as a result of random fluctuations. Our simple theory neglects those fluctuations, assuming instead that Q_{SI} is constant. The fluctuations would be less important in significantly larger networks. Therefore, we would expect the predictions of inequality 8.5 to be more accurate in larger networks.

For the parameter values of Figure 9A, Figure 11A illustrates the transition from low, inconsequential levels of noise in the E-cells to disruptive levels. The figure shows quantities $\rho_E \in [0, 1]$ and $\rho_I \in [0, 1]$, measuring the regularity of the spiking of the E- and I-cells, plotted as functions of the noise frequency ν_{SE}. The precise definitions of ρ_E and ρ_I are given in appendix B. The closer ρ_E and ρ_I are to 1, the more regular is the rhythm. The figure shows that the regularity of the rhythm is lost abruptly as ν_{SE} is raised above 6.

If in fact it is correct that the rhythm in Figure 9B is disrupted essentially as a result of too much drive to the I-cells, then it ought to be possible to restore the rhythm by lowering g_{EI}. Indeed, this is the case. When g_{EI} is lowered to 0.02, the rhythm shown in Figure 9C is obtained.

8.2.2 At Gamma frequency, I→I Synapses Greatly Reduce Sensitivity to Noise in the E-Cells. Figures 5B and 5D show that in large portions of parameter space, I→I synapses greatly enlarge the amount of drive to the I-cells that PING rhythms can withstand before breaking down as a result of phase walkthrough. To confirm this by simulation, we use the parameter values of Figure 9A, but replace $g_{II} = 0$ by $g_{II} = g_{IE}$. The resulting rhythm is astonishingly insensitive to noisy spiking in the E-cells. Formula 8.8 predicts that the rhythm should survive for $\nu_{SE} \leq 77$. Figure 9D shows a simulation with $\nu_{SE} = 70$. The spike time rastergram for the E-cells looks quite noisy, of course, but the rhythm is still visible. (Because of stochastic fluctuations, the rhythm would not, in reality, remain intact if ν_{SE} were equal to 77.)

8.2.3 Sensitivity to Noise in the E-Cells Increases as the Rhythm Slows Down. We now present numerical simulations illustrating that slower PING rhythms are more sensitive to noisy spiking of the E-cells, as predicted by Figure 5A and formulas 8.5 and 8.8. Figure 9E shows a slow PING rhythm disrupted by a small amount of stochastic spiking in the E-cells. (Notice that the time window shown in Figures 9E and 9F is four times longer than that shown in Figures 9A–9D.) The parameter values of Figure 9E are those of Figure 9A, except that I_E has been reduced from 0.1 to 0.003. The frequency of the resulting PING rhythm is about 10. Formula 8.5 predicts that this rhythm should be abolished by random spiking in the E-cells at an average frequency of about $\nu_{SE} = 0.76$. Indeed, phase walkthrough occurs

for $\nu_{SE} = 0.5$ already. This is shown in Figure 9E. Thus, phase walkthrough again occurs at a (somewhat) lower value of ν_{SE} than predicted by our theory. As before, the discrepancy is due primarily to the stochastic fluctuations in the drive to the I-cells generated by the random spiking of the E-cells.

For this case, Figure 11B illustrates the transition from nearly inconsequential levels of noise in the E-cells to disruptive levels. The regularity of the rhythm is lost abruptly as ν_{SE} is raised above 0.4.

It is not surprising that the maximum allowable value of ν_{SE} decreases as ν_P decreases. For instance, if the maximum allowable value of ν_{SE} is 6 for $\nu_P = 40$ (see Figure 11A), one might expect it to be four times smaller for $\nu_P = 10$. What is surprising is that it is not 4 but 16 times smaller (see Figure 11B). This is in agreement with inequality 8.5, as the right-hand side of that inequality, for $I_I = 0$, is proportional to $(\nu_P/1000)^2$, not to $\nu_P/1000$.

8.2.4 At Subgamma Frequencies, Careful Parameter Tuning Can Reduce Sensitivity to Noise in the E-Cells. At low frequencies, I→I synapses do not help much. Inequality 8.8 predicts that even with $g_{II} = g_{IE}$, phase walkthrough of the I-cells will occur as soon as $\nu_{SE} > 2.3$. However, the robustness of the rhythm can be enhanced by reducing g_{EI}. Figure 9F shows a simulation in which the parameter values are as in Figure 9E, except $g_{II} = g_{IE}$, $g_{EI} = 0.01$, and $\nu_{SE} = 7$.

9 Suppression of the E-Cells Resulting from Stochastic Spiking of the I-Cells

In this section, we consider the effects of random spiking of the I-cells, for instance, as a result of stochastic external input. We show that noisy spiking of the I-cells disrupts PING rhythms by causing suppression of the E-cells. We give an approximate analysis of the conditions under which noise in the I-cells results in suppression of the E-cells. As in section 8, our analysis is not very accurate quantitatively, again because it neglects statistical fluctuations that are significant at least in small networks. It does reveal that the crucial quantity here is the product $r\tau_I$: the larger $r\tau_I$, the less noisy spiking in the I-cells can be tolerated.

In our simulations, we enforce random spiking of the I-cells in the same way in which we enforced random spiking of the E-cells in section 8. In analogy with section 8, T_{SI} denotes the expected time between two random spikes of a given I-cell, and

$$\nu_{SI} = 1000/T_{SI} \,. \tag{9.1}$$

Figures 10B and 10F (discussed in detail shortly) show examples of rhythms that persist in spite of random spiking in the I-cells. When an I-cell spikes out of order, it is temporarily out of synchrony with the bulk of the I-cells. However, it is brought back into synchrony when the next

population spike of the E-cells prompts a population spike of the I-cells.

9.1 Analysis. The low-frequency random spiking of some of the I-cells between population spikes generates inhibitory synaptic drive to the E-cells. If each E-cell receives input from sufficiently many I-cells, this drive is nearly constant. If it is strong enough, it leads to suppression of the E-cells, and thereby abolishes the rhythm (see Figure 10D).

A necessary and sufficient condition for the E-cells to escape suppression is

$$\overline{s} < \frac{1}{r}\,, \tag{9.2}$$

with

$$\overline{s} = \frac{1}{T_{SI}} \int_0^{T_{SI}} e^{-t/\tau_I}\, dt = \frac{1 - e^{-T_{SI}/\tau_I}}{T_{SI}/\tau_I} \tag{9.3}$$

(see equation 6.3, which is the same as equation 9.2, and equation 2.19, which is nearly the same as equation 9.3, the only difference being that the deterministic interspike interval T_I in equation 2.19 has been replaced by the expected interspike interval T_{SI} in equation 9.3). We are interested in low-frequency random spiking of the I-cells, and thus assume $T_{SI} \gg \tau_I = 10$. Therefore, the term e^{-T_{SI}/τ_I} in equation 9.3 is negligible, and condition 9.2 becomes

$$\frac{\tau_I}{T_{SI}} < \frac{1}{r}\,,$$

or, equivalently, using equation 9.1,

$$\frac{\nu_{SI}}{1000} < \frac{1}{r\tau_I}\,. \tag{9.4}$$

This formula shows that the sensitivity of PING rhythms to random spiking in the I-cells depends on the size of $r\tau_I$.

9.2 Numerical Examples.

9.2.1 Too Much Noise in the I-Cells Leads to Suppression of the E-Cells. Figure 10A shows, once more, the simulation of Figure 9A. Figure 10B shows the result of adding random spiking of the I-cells at frequency $\nu_{SI} = 25$ to the simulation in Figure 10A. The noisy spiking in the I-cells slows the rhythm (as it should, since it inhibits the E-cells), but it does not disrupt it. At $\nu_{SI} = 30$ (not shown in Figure 10), the time intervals between population spikes become irregular. Formula 9.4 predicts that suppression of the E-cells should occur for $\nu_{SI} > 33$, approximately. In our simulations, even for $\nu_{SI} = 40$, the

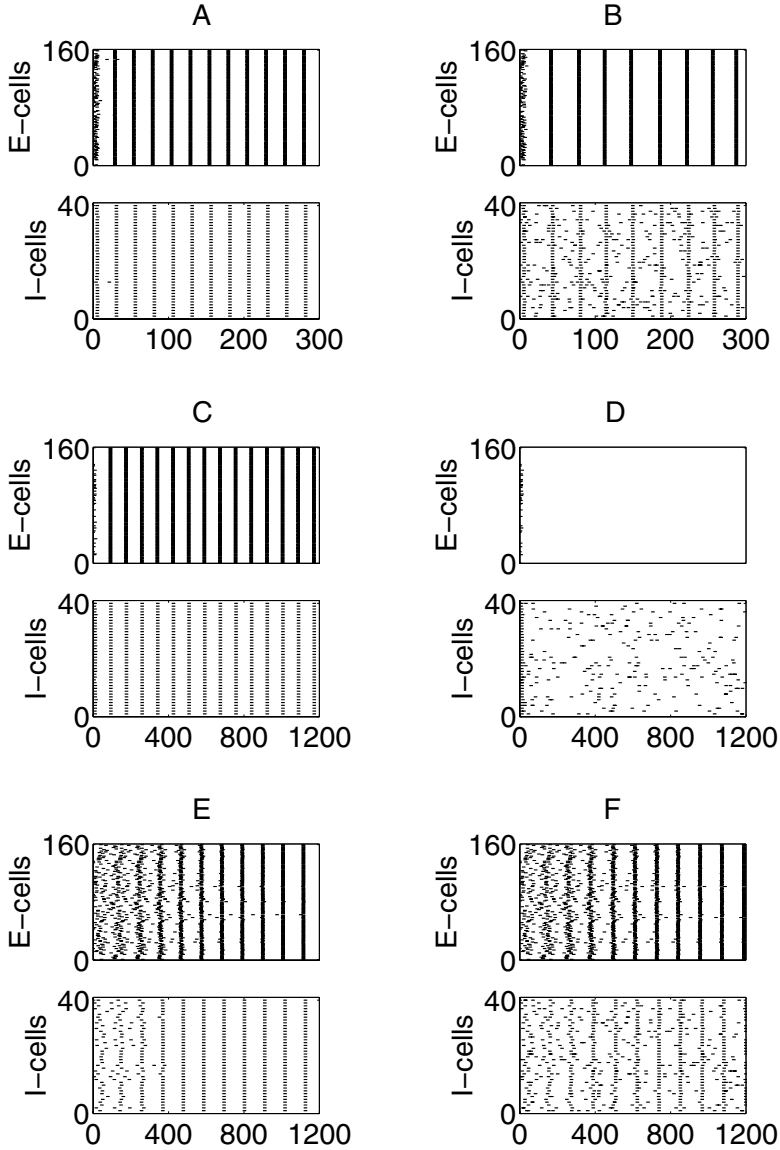

Figure 10: (A) Gamma frequency PING rhythm with $r = 3$ ($g_{EI} = 0.05$, $g_{IE} = 0.2$, $g_{II} = 0$, $I_E = 0.1$, $I_I = 0$). (B) Considerable noise in the I-cells can be withstood by this rhythm. (C) Low-frequency PING rhythm with $r = 60$ ($I_E = 0.005$; all other parameters as in *A*). (D) This rhythm is highly sensitive to noise in the I-cells. (E) Low-frequency PING rhythm with $r = 3$ ($I_E = 0.001$, $g_{IE} = 0.002$; all other parameter values as in *A*). (F) Considerable noise in the I-cells can be withstood by this rhythm.

E-cells are not suppressed, but the intervals between population spikes of the E-cells are long and quite irregular. Thus, the regularity of the rhythm is disrupted earlier (for smaller ν_{SI}) than predicted by our theory, but complete suppression of the E-cells occurs later (for larger ν_{SI}) than predicted by our theory. This discrepancy between our theory and the numerical simulations is not hard to understand. In our theory, statistical fluctuations in the strength of inhibition received by the E-cells are neglected. These fluctuations make the rhythm irregular earlier (for smaller ν_{SI}) than predicted by our theory. When the inhibition happens to be stronger than average, the E-cells are delayed, and when it happens to be weaker than average, the E-cells spike earlier. However, statistical fluctuations cause complete suppression of the E-cells to occur later (for larger ν_{SI}) than predicted by our theory. Even when inhibition is strong enough, on the average, to suppress the E-cells, there are time windows when it happens to fall below the threshold required for suppression. Population spikes of the E-cells may occur during those time windows.

For the parameter values of Figure 10A, Figure 11C illustrates the transition from low, inconsequential levels of noise in the I-cells to disruptive levels. The figure shows the regularity measures ρ_E and ρ_I (see appendix B) plotted as functions of ν_{SI}.

9.2.2 Sensitivity to Noise in the I-Cells Increases as Drive to the E-Cells Weakens. We lower I_E to 0.005. The frequency of the PING rhythm decreases to about 12, and r rises to 60. Figure 10C shows the rhythm without any stochastic spiking. (Notice that the time window shown in parts C–F of Figure 10 is four times longer than that shown in parts A and B.) Adding stochastic spiking of the I-cells at average frequency $\nu_{SI} = 5$, the E-cells are suppressed, and thereby the rhythm is abolished (see Figure 10D).

For the parameter values of Figure 10C, Figure 11D illustrates the transition from low, inconsequential levels of noise in the I-cells to disruptive levels. Note that the value of I_E is 20 times smaller in Figure 11D than in Figure 11C, and the value of r is therefore 20 times larger. According to inequality 9.4, the maximum frequency of noise in the I-cells that the rhythm can withstand should therefore be 20 times smaller in Figure 11D than in Figure 11C. Indeed, this is approximately the case.

9.2.3 For Weakly Driven E-Cells, Careful Parameter Tuning Can Reduce Sensitivity to Noise in the I-Cells. We have mentioned that PING rhythms with low values of I_E can be made fairly noise insensitive by lowering g_{IE} proportionally, ensuring that r does not become too large. To illustrate this, we lower I_E even further, to 0.001, but also lower g_{IE} to 0.002, bringing the value of r back to 3, as in Figure 10A. For reasons discussed in the next paragraph, we also use a smaller value of g_{EI} here: $g_{EI} = 0.005$. The frequency of the resulting rhythm is approximately 8 (see Figure 10E). Remarkably, the rhythm in Figure 10E survives stochastic spiking of the I-cells at frequency

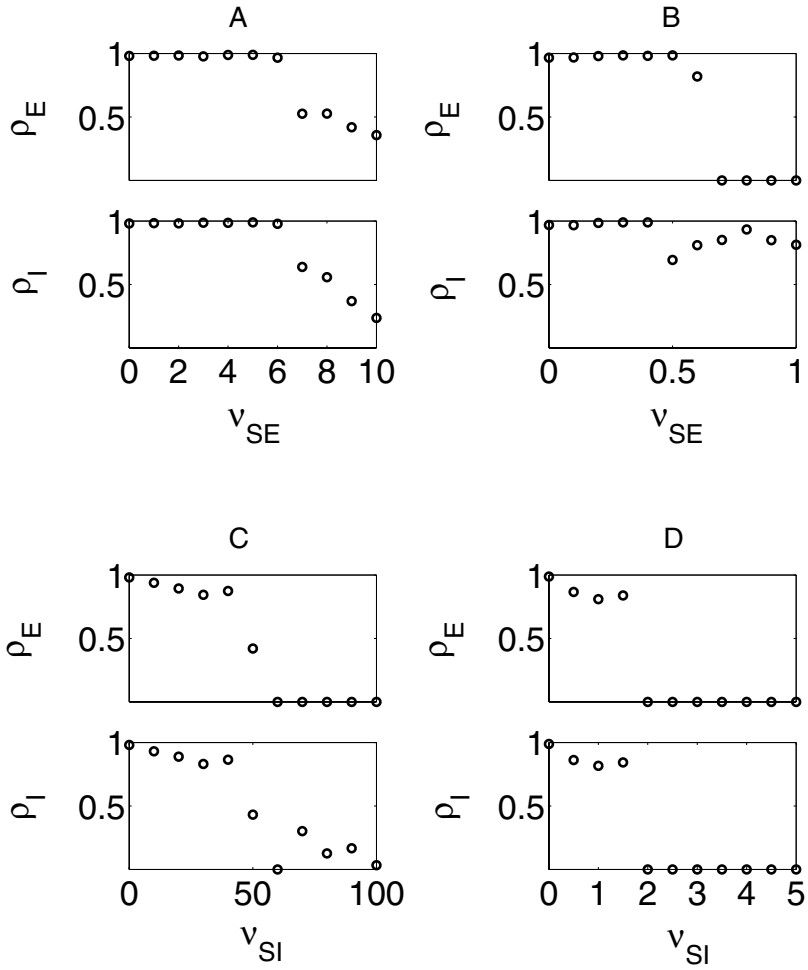

Figure 11: Regularity measures ρ_E and ρ_I (defined in appendix B) as functions of noise frequency. (A) At gamma frequency (40 Hz), the rhythm can withstand 6 Hz noise in the E-cells. (B) At four times lower frequency (10 Hz), it can withstand no more than 0.4 Hz noise in the E-cells. (C) At gamma frequency (40 Hz), the regularity of the rhythm is lost if the frequency of the noise in the I-cells is greater than 40 Hz. (D) When I_E is reduced twenty-fold, the rhythm can withstand no more than 1.5 Hz noise in the I-cells.

5 (see Figure 10F). This is a result of the moderate (not very large) value of r.

In the preceding simulation, we used a reduced value of g_{EI}. In general, for small g_{IE}, the PING rhythm is more rapidly established if g_{EI} is small as well. (Of course, g_{EI} must still be large enough for a population spike of the E-cells to trigger a population spike of the I-cells.) Section 8 suggests the following heuristic explanation of this numerical observation. In the initial phases of the simulation, before the rhythm is established, the population spikes are fuzzy (see, for instance, the beginning of the simulation in Figure 10E). If g_{IE} is small, there is a considerable amount of nearly asynchronous activity of the E-cells between activity peaks. This activity results in nearly tonic drive to the I-cells, which may result in premature spiking of some of the I-cells, and may therefore make it more difficult for the rhythm to be established. Lowering g_{EI} reduces this effect.

9.2.4 Effects of I→I Synapses. We have used $g_{II} = 0$ throughout this section. As pointed out in earlier sections, I→I synapses generally stabilize PING rhythms by slowing disruptive spiking in the I-cells. However, in the experiments presented here, the disruptive spiking in the I-cells is forced, regardless of the value of g_{II}. As a result, if g_{II} were set to g_{IE}, the results presented in this section would remain virtually unchanged. If the random spiking were instead generated by weaker random input pulses, not necessarily always inducing immediate spiking, then I→I synapses would indeed counteract the suppression of the E-cells by the I-cells.

10 Simulations Including Sparse Connectivity and Heterogeneity

In this section, we present some numerical simulations including sparse connectivity and heterogeneity. We sparsen the connectivity as follows. The possible synaptic connections are considered one at a time. Each possible connection is removed with probability 0.5. If it is retained, its strength is doubled. For instance, the strength of an I→E connection is 0 with probability 0.5, and $2g_{IE}/N_I$ with probability 0.5.

This is a moderate degree of sparseness. However, in earlier work (Börgers & Kopell, 2003), we showed that the effect of sparseness on the coherence of a PING rhythm is determined not by the fraction p of connections retained, but by $pN_E/(1-p)$ and $pN_I/(1-p)$. For instance, in a 10 times larger network (i.e., in a network of 1600 E-cells and 400 I-cells), we would get approximately the same effect if we removed connections with probability 10/11 and strengthened the retained connections eleven-fold. (Note that $p/(1-p) = 1/10$ when $p = 1/11$.)

In addition to sparseness, we introduce 20% heterogeneity in synaptic strengths. For instance, the strength of a given retained I→E synapse is not precisely $2g_{IE}/N_I$, but rather a gaussian random number with mean $2g_{IE}/N_I$ and standard deviation $0.4g_{IE}/N_I$. (This random number is negative with

very small but positive probability. If our program draws a negative strength for one of the synapses, the strength of that synapse is reset to zero.) Thus, g_{IE}, g_{EI}, and g_{II} are no longer the total synaptic strengths, but they are (very close to) the expected total synaptic strengths.

We also introduce 20% heterogeneity in the external drive to the E-cells. That is, the external drive received by a given E-cell is not precisely I_E, but rather a gaussian random number with mean I_E and standard deviation $0.20I_E$. Thus, I_E is no longer the external drive to each E-cell, but it is the expected external drive to each E-cell. Similarly, we introduce 20% heterogeneity in the external drive to the I-cells.

Finally, all cells are forced to spike at random times at average frequencies ν_{SE} (for the E-cells) and ν_{SI} (for the I-cells).

At gamma frequency, PING is robust to heterogeneity, random connectivity, and noisy external drives. Figure 12A shows the results of a simulation with

$$g_{IE} = 0.2, \quad g_{EI} = 0.05, \quad g_{II} = 0.2, \quad I_E = 0.1 \quad (\nu_E \approx 101), \quad I_I = 0.05, \quad \nu_{SE} = 5, \quad \nu_{SI} = 5.$$

Figure 12B shows, for the same simulation, quantities $s_E = s_E(t)$ and $s_I = s_I(t)$ measuring the average strength of excitatory and inhibitory synapses (see appendix B for precise definitions). The rhythm is clearly detectable in Figures 12A and 12B. Its frequency is approximately 40.

Even with heterogeneity and random connectivity, it is possible to obtain PING rhythms at subgamma frequencies, but careful parameter tuning is required. As discussed in section 8.2, one should lower g_{EI}, to avoid phase walkthrough as a result of the drive to the I-cells resulting from noisy activity of the E-cells. However, one cannot lower g_{EI} too much, since the I-cells must respond promptly to population spikes of the E-cells. As discussed in section 9, one should lower both I_E and g_{IE} proportionally, keeping r constant. This avoids making the rhythm vulnerable to suppression of the E-cells by noisy spiking of the I-cells.

The parameter values

$$g_{IE} = 0.004, \quad g_{EI} = 0.004, \quad g_{II} = 0.004, \quad I_E = 0.001 \quad (\nu_E \approx 10), \quad I_I = 0.0005, \nu_{SE} = 2, \quad \nu_{SI} = 2$$

yield a PING rhythm at frequency $\nu_P \approx 8$ in the presence of sparse connectivity, heterogeneity, and noise. Sparseness and heterogeneity are introduced as described earlier. Figure 12C shows the spike times, and Figure 12D shows s_E and s_I for the same simulation. (Notice that the time window shown in Figures 12C and 12D is five times longer than that shown in Figures 12A and 12B.)

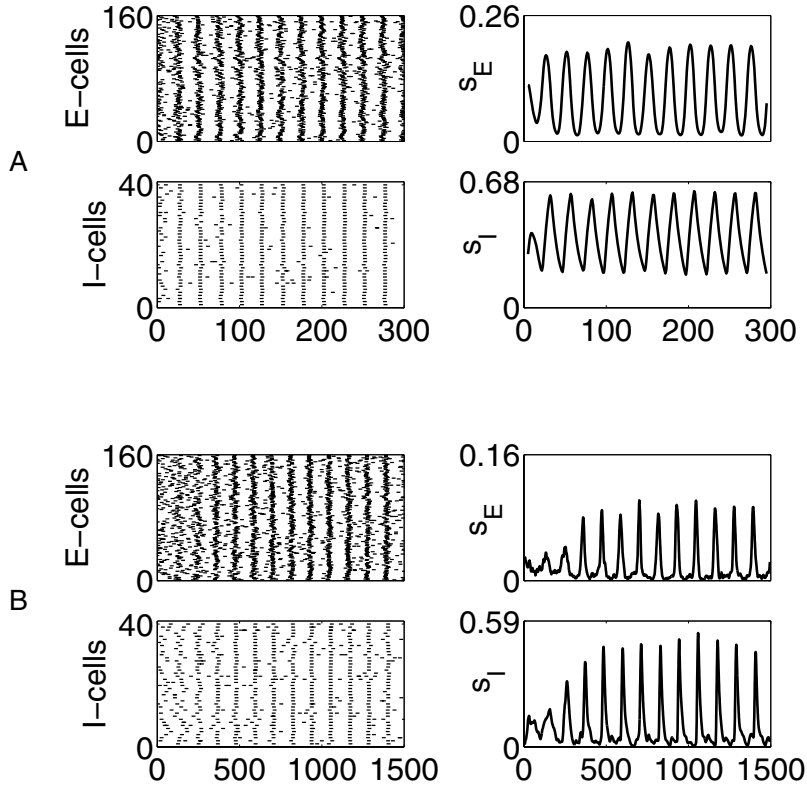

Figure 12: Sparse connectivity, heterogeneity, and noise do not necessarily abolish PING rhythm, either at gamma frequency or—with carefully tuned parameter values—at lower frequencies. (A) Gamma frequency PING rhythm ($g_{EI} = 0.05$, $g_{IE} = 0.2$, $g_{II} = 0.2$, $I_E = 0.1$, $I_I = 0.05$); spike times (left panel), and s_E and s_I as defined in appendix B (right panel). (B) Low-frequency PING rhythm ($g_{EI} = 0.004$, $g_{IE} = 0.004$, $g_{II} = 0.004$, $I_E = 0.001$, $I_I = 0.0005$); spike times (left panel), and s_E and s_I (right panel).

11 The Frequency Range in Which PING is Robust

A major theme of this letter has been that PING rhythms at low frequencies, significantly below the gamma range, are easily abolished by noise, unless the parameter values are tuned very carefully. In fact, there is also a sense in which PING rhythms at high frequencies, above the gamma range, are not robust.

We remarked earlier that one typically needs $r \geq 3$ for synchronization in the presence of 20% heterogeneity in network parameter values. Combining

this with equation 3.15, and recalling $q \leq 1$, we find

$$T_P \geq (\ln 3)\,\tau_I \approx 1.1\,\tau_I\ .$$

If $\tau_I = 10$, then $T_P \geq 11$, which approximately means $\nu_P \leq 91$. Thus, in the presence of significant heterogeneity, PING rhythms cannot have a frequency above the gamma range.

This argument is, of course, far from precise. In particular, nothing is really special about the value $r = 3$. Nevertheless, we do believe that the argument is correct in essence. In more intuitive language, when one attempts to drive the frequency of a PING rhythm above the gamma range by raising drive to the E-cells, one must also raise the strength of the I→E synapses in order to maintain synchronization. The rise in the strength of the I→E synapses brings the frequency back into the gamma range.

12 Summary and Discussion

We have described and analyzed two distinct ways in which too much external drive to the I-cells can disrupt PING rhythms: The I-cells may synchronize, but get ahead of the E-cells (phase walkthrough of the I-cells), or the I-cells may not synchronize, and their activity may keep the E-cells from spiking altogether (suppression of the E-cells). Our analysis of the effects of deterministic drive to the I-cells casts light on the effects of stochastic drive to the E- or I-cells. If there is too much noisy spiking activity in the E-cells, the resulting rise in excitatory drive to the I-cells may lead to phase walkthrough; too much noisy spiking in the I-cells may result in suppression of the E-cells. I→I synapses reduce the spiking frequency of the I-cells, counteracting phase walkthrough of the I-cells, suppression of the E-cells, and the effects of noisy external drive on both I- and E-cells, and thereby enhancing the robustness of the rhythm.

Our analysis also shows why PING rhythms are most robust when their frequency lies in the gamma range. Above the gamma range, synchronization breaks down easily when the E-cell population is heterogeneous. As the frequency is lowered, on the other hand, PING becomes increasingly sensitive to noisy spiking of the E-cells, and—unless the strength of the inhibitory synapses and the drive to the E-cells are calibrated carefully—more sensitive to noisy spiking of the I-cells as well.

Gutkin and Ermentrout (1998) showed that noise sensitivity of type I model neurons is greater at lower frequencies than at higher frequencies, (see in particular Figure 6B of their article). Our point about noise sensitivity and frequency may seem similar at first but is in fact quite different. Gutkin and Ermentrout showed for a *single* theta neuron that *noisy* drive has a more severe effect when the *intrinsic* frequency of the neuron is low than when it is high. We have shown for an E/I *network* that the *tonic* component of the drive to the I-cells created by noisy spiking in the E-cells has a more severe effect when the *population* frequency is low than when it is high.

We conclude with a brief discussion of the relation of our work to previous work on synchronization in networks of model neurons. Much of this work has addressed purely excitatory networks (e.g., Peskin, 1975; Mirollo & Strogatz, 1990; Somers & Kopell, 1993; Hansel, Mato, & Meunier, 1995; Crook, Ermentrout, & Bower, 1998; Bose, Kopell, & Terman, 2000; van Vreeswijk & Hansel, 2001; Acker, Kopell, & White, 2003), purely inhibitory networks (e.g., Wang & Rinzel, 1992; Golomb & Rinzel, 1993; Skinner, Kopell, & Marder, 1994; Chow, 1998; Chow, White, Ritt, & Kopell, 1998; Terman, Kopell, & Bose, 1998; White, Chow, Ritt, Soto-Tervino, & Kopell, 1998; Brunel & Hakim, 1999), or pairs of neurons that are either both excitatory, or both inhibitory (e.g. van Vreeswijk, Abbott, & Ermentrout, 1994; Kopell & Ermentrout, 2002). Synchronization in networks including both excitatory and inhibitory model neurons has been studied widely as well (e.g., Wang, Golomb, & Rinzel, 1995; Ermentrout & Kopell, 1998; Brunel, 2000a, 2000b; Whittington et al., 2000; Tiesinga et al., 2001; Hansel & Mato, 2001; van Vreeswijk & Hansel, 2001; Börgers & Kopell, 2003; Hansel & Mato, 2003). For more complete references, see Kopell and Ermentrout (2002) or Hansel and Mato (2003).

Much of the work on (a)synchrony in neuronal networks has focused on states of asynchronous spiking and ways in which such states can lose stability (Abbott & Van Vreeswijk, 1993; Gerstner & van Hemmen, 1993; Hansel et al., 1995; Gerstner, 2000; Neltner Hansel, Mato, & Meunier, 2000; van Vreeswijk, 2000; Hansel & Mato, 2003). In this letter, we have taken a complementary point of view, focusing on states of nearly synchronous spiking, asking for which parameter values such states exist and how sensitive they are to changes in parameter values and noise.

Hansel and Mato (2003) gave a comprehensive analysis of the bifurcations by which asynchronous states can lose stability in networks of excitatory and inhibitory neurons. They identified four codimension 1 bifurcations, of which three lead to oscillatory behavior. One of these (the one associated with crossing the curve L4 in Figure 11 of Hansel and Mato, 2003) corresponds to the emergence of PING and another (associated with the curve L2 in the same figure) to the emergence of ING. In drawing their phase diagrams, Hansel and Mato varied the strengths of synaptic conductances while adjusting external drives to keep the average firing rates of the E- and I-cell populations constant. By contrast, we have treated synaptic strengths and external drives as independent parameters. This difference in point of view complicates direct comparisons between the results of Hansel and Mato and ours. In particular, the lower panel of Figure 11 of Hansel and Mato shows that in a certain sense, I→I synapses counteract PING. For stronger I→I synapses, stronger coupling between the E- and I-cells is needed for the transition from asynchrony to PING (crossing the L4 boundary). At first sight, this appears to contradict our conclusion that I→I synapses *promote* PING by protecting against phase walkthrough of the I-cells and suppression of the E-cells. However, in fact, there is no contra-

diction, since different points in the phase plane depicted by Hansel and Mato correspond to different external drives.

The frequency of PING oscillations was analyzed in a recent paper by Brunel and Wang (2003). We note that their study was concerned with oscillations driven by noisy input, whereas in this article, we have focused on oscillations driven by deterministic input (and, in some cases, disrupted by a noisy input component). However, not all discrepancies between their results and ours can plausibly be explained by this difference. For instance, equation 18 of Brunel and Wang (2003) determines the population frequency of the oscillation for E/I networks without E→E and I→I synapses. According to this equation, the frequency depends on synaptic delay, rise, and decay times. In our simulations, there are no synaptic delays, and synaptic rise times are very short. Furthermore, numerical results (not shown here) indicate that shortening the synaptic rise times much further has little impact on the results of our simulations, and the same holds even when the rhythm is driven by noise instead of deterministic tonic drive. This motivates consideration of the limit of equation 18 of Brunel and Wang (2003) as the synaptic delay and rise times tend to zero. Doing this, one finds the prediction that the population oscillation frequency should tend to infinity—in stark discrepancy with our numerical results. The reason for this and other discrepancies between the results of Brunel and Wang and ours remains to be determined. An important difference between the study of Brunel and Wang and ours lies in the choice of membrane time constants for the excitatory neurons. Brunel and Wang used linear integrate-and-fire neurons with time constants equal to 10 ms for inhibitory neurons and 20 ms for excitatory ones. Significantly shorter membrane time constants are believed to be appropriate for neocortical pyramidal neurons in vivo during high ongoing activity (Destexhe & Paré, 1999; Destexhe, Rudolph, & Paré, 2003).

For theta neurons, as for real cortical neurons, the membrane time "constant" is not actually a constant, but depends on external input. In our simulation of gamma rhythms, the E-cells typically have rather short membrane time constants (on the order of few milliseconds) shortly after receiving input from the I-cells; this is what makes the stable river in Figure 3A strongly attracting and allows for synchronization of the E-cells within one gamma cycle.

Appendix A: The Impact of Synchrony and Asynchrony on Downstream Effects

In computing the suppression boundary, we assumed that the activity of the I-cells was completely asynchronous. The rationale for this assumption was that asynchrony maximizes the downstream effect of an assembly of inhibitory neurons. In this appendix, we prove a precise statement to this effect. We also prove a precise statement showing that synchrony maximizes

the downstream effect of an assembly of excitatory neurons. In contrast with the main portion of this article, we use the linear integrate-and-fire model here. We have not so far generalized these results to the theta model.

We begin with a precise version of the following claim. If N periodic current inputs succeed in making an integrate-and-fire neuron spike, then the same inputs would also succeed in making the neuron spike if they were synchronized.

Theorem 1. *Let $\varphi \geq 0$ be periodic function with period T, and let $t_1, ..., t_N \in [0, T)$. Let $\tau > 0$, and consider the initial value problems*

$$\begin{aligned} \frac{dV}{dt} &= -\frac{V}{\tau} + \sum_{i=1}^{N} \varphi(t - t_i) \\ V(0) &= 0 \end{aligned}$$

and

$$\begin{aligned} \frac{d\hat{V}}{dt} &= -\frac{\hat{V}}{\tau} + N\varphi(t). \\ \hat{V}(0) &= 0 \end{aligned}$$

Then

$$\sup_{t \geq 0} \hat{V}(t) \geq \sup_{t \geq 0} V(t) \, .$$

Proof. Denote by $V(V_0; t_1, ..., t_N; t)$ the solution of

$$\begin{aligned} \frac{dV}{dt} &= -\frac{V}{\tau} + \sum_{i=1}^{N} \varphi(t - t_i). \\ V(0) &= V_0. \end{aligned}$$

In general,

$$V(V_0; t_1, ..., t_N; t) = \int_0^t \left(\sum_{i=1}^{N} \varphi(s - t_i) \right) e^{(s-t)/\tau} \, ds + V_0 e^{-t/\tau} \, . \qquad \text{(A.1)}$$

To find solutions with period T, we define $V_{0,per} > 0$ to be the solution of

$$\int_0^T \left(\sum_{i=1}^{N} \varphi(s - t_i) \right) e^{(s-T)/\tau} \, ds + V_{0,per} e^{-T/\tau} = V_{0,per} \, .$$

We write

$$V_{per}(t_1, ..., t_N; t) = V(V_{0,per}; t_1, ..., t_N; t) .$$

From equation A.1,

$$V(0; t_1, ..., t_N; t) < V(V_{0,per}; t_1, ..., t_N; t)$$

for all t, but

$$\lim_{t\to\infty} \left| V(0; t_1, ..., t_N; t) - V(V_{0,per}; t_1, ..., t_N; t) \right| = 0 .$$

Therefore,

$$\sup_{t\geq 0} V(0; t_1, ..., t_N; t) = \sup_{t\geq 0} V_{per}(t_1, ..., t_N; t) .$$

We denote by $\hat{V}_{per}$ the uniquely determined solution with period T of

$$\frac{d\hat{V}_{per}}{dt} = -\frac{\hat{V}_{per}}{\tau} + \varphi(t) .$$

Then

$$V_{per}(t_1, ..., t_N; t) = \sum_{i=1}^{N} \hat{V}_{per}(t - t_i) .$$

Therefore,

$$\sup_{t\geq 0} V_{per}(t_1, ..., t_N; t) \leq N \sup_{t\geq 0} \hat{V}_{per}(t) ,$$

with "=" if $t_i = 0$ for all i. Therefore,

$$\begin{aligned} \sup_{t\geq 0} V(0; t_1, ..., t_N; t) &= \sup_{t\geq 0} V_{per}(t_1, ..., t_N; t) \\ &\leq N \sup_{t\geq 0} \hat{V}_{per}(t) \\ &= \sup_{t\geq 0} V_{per}(0, ..., 0; t) \\ &= \sup_{t\geq 0} V(0; 0, ..., 0; t). \end{aligned}$$

This proves the assertion.

We next show that asynchrony minimizes the downstream effect of an assembly of excitatory neurons. More precisely, we will show that if a given asynchronous excitatory synaptic input succeeds in making an integrate-and-fire neuron spike, then the same input, delivered phasically with a period T, will also succeed in making the neuron spike.

Theorem 2. *Let $I \in \mathbb{R}$, $\tau > 0$, $V_{rev} \in \mathbb{R}$ (think of V_{rev} as the reversal potential of an* excitatory *synapse), and let $g = g(t) \geq 0$ be a function with period T. Define $V = V(t)$ by*

$$\begin{aligned} \frac{dV}{dt} &= -\frac{V}{\tau} + I + g(V_{rev} - V) \\ V(0) &= 0 \, . \end{aligned}$$

Let

$$\overline{g} = \frac{1}{T} \int_0^T g(t)dt \, .$$

Define $\overline{V} = \overline{V}(t)$ by

$$\begin{aligned} \frac{d\overline{V}}{dt} &= -\frac{\overline{V}}{\tau} + I + \overline{g}(V_{rev} - \overline{V}) \\ \overline{V}(0) &= 0 \, . \end{aligned}$$

Then

$$\sup_{t \geq 0} \overline{V}(t) \leq \sup_{t \geq 0} V(t) \, .$$

Proof. If $\sup_{t \geq 0} V(t) = \infty$, then we have nothing to prove, so assume $\sup_{t \geq 0} V(t) < \infty$.

$$\begin{aligned} \frac{dV}{dt} &= -\frac{V}{\tau} + I + g(t)(V_{rev} - V) \\ &\geq -\frac{\sup\limits_{t \geq 0} V(t)}{\tau} + I + g(t) \left(V_{rev} - \sup_{t \geq 0} V(t) \right) . \end{aligned} \tag{A.2}$$

The right-hand side of this inequality is a periodic function of t and a lower bound on dV/dt. The assumption $\sup_{t \geq 0} V(t) < \infty$ then implies that the average of the right-hand side of equation A.2 is ≤ 0:

$$-\frac{\sup\limits_{t \geq 0} V(t)}{\tau} + I + \overline{g} \left(V_{rev} - \sup_{t \geq 0} V(t) \right) \leq 0 \, .$$

This means that $d\overline{V}/dt$ would be ≤ 0 if $\overline{V}$ ever reached $\sup_{t\geq 0} V(t)$. So $\overline{V}$ cannot exceed $\sup_{t\geq 0} V(t)$. This proves the assertion.

Thinking of V_{rev} as the reversal potential of an inhibitory synapse, one can reinterpret the statement just proved as follows. If a given inhibitory synaptic input suppresses an integrate-and-fire neuron, then the same input, delivered asynchronously, will also suppress the neuron. That is, asynchrony maximizes the downstream effect of an assembly of inhibitory neurons.

Appendix B: A Measure of Regular Rhythmicity

We associate synaptic gating variables with the presynaptic neurons (see section 2.2). Let $s_{E,i}$ denote the synaptic gating variable associated with ith E-cell, $1 \leq i \leq N_E$, and let $s_E(t)$ be the average of $s_{E,i}$ over $i \in \{1, 2, ..., N_E\}$ and over the time interval $[t-5, t+5]$. We approximate the time average using the trapezoid method. The time averaging is needed in some of our noisier simulations (for instance, those of Figure 12) to eliminate small random fluctuations that would make automatic detection of the underlying rhythm difficult.

We define

$$s_{E,min} = \min_t s_E(t) \ , \quad s_{E,max} = \max_t s_E(t) \ , \quad \text{and} \quad s_{E,av} = \frac{s_{E,min} + s_{E,max}}{2} \ .$$

The minimum and maximum are taken over the second half of the simulation time interval to avoid the effects of initial transients. We consider those times t in the second half of the simulation time interval at which s_E changes from values below $s_{E,av}$ to values above $s_{E,av}$. We denote these times by

$$t_{E,1} < t_{E,2} < ... < t_{E,n_E} \ .$$

Our measure of (regular) rhythmicity is

$$\rho_E = \begin{cases} \dfrac{\min(t_{E,i+1} - t_{E,i})}{\max(t_{E,i+1} - t_{E,i})} & \text{if } n_E \geq 3 \ , \\ 0 & \text{otherwise} \ . \end{cases}$$

Here the minimum and maximum are taken over $i \in \{1, 2, ..., n_E - 1\}$. Clearly $\rho_E \in [0, 1]$; the closer ρ_E is to 1, the more regular is the rhythm.

To visualize and measure rhythmicity of the I-cells, $s_I(t)$ and ρ_I are defined analogously.

Acknowledgments

We are grateful to Steve Epstein for reading the manuscript and providing helpful criticism. We also thank the referees for their detailed and thoughtful comments, which led to several improvements in the article. C.B. is

supported by NSF grant DMS-0418832. N.K. is supported by NSF grant DMS-9706694 and NIH grant MH47150.

References

Abbott, L. F., & van Vreeswijk, C. (1993). Asynchronous state in networks of pulse-coupled oscillators. *Phys. Rev. E, 48*, 1483–1490.

Acker, C., Kopell, N., & White, J. (2003). Synchronization of strongly coupled excitatory neurons: Relating network behavior to biophysics. *J. Comp. Neurosci., 15*, 71–90.

Börgers, C., & Kopell, N. (2003). Synchronization in networks of excitatory and inhibitory neurons with sparse, random connectivity. *Neural Comp., 15*(3), 509–539.

Bose, A., Kopell, N., & Terman, D. (2000). Almost synchronous solutions for pairs of neurons coupled by excitation. *Physica D, 140*, 69–94.

Brunel, N. (2000a). Dynamics of sparsely connected networks of excitatory and inhibitory spiking neurons. *J. Comp. Neurosci., 8*, 183–208.

Brunel, N. (2000b). Phase diagrams of sparsely connected networks of excitatory and inhibitory spiking neurons. *Neurocomputing, 32*, 307–312.

Brunel, N., & Hakim, V. (1999). Fast global oscillations in networks of integrate-and-fire neurons with low firing rates. *Neural Comp., 11*, 1621–1671.

Brunel, N., & Wang, X.-J. (2003). What determines the frequency of fast network oscillations with irregular neural discharges? I. Synaptic dynamics and excitation-inhibition balance. *J. Neurophysiol., 90*, 415–430.

Charpak, S., Gähwiler, B. H., Do, K. Q., & Knöpfel, T. (1990). Potassium conductances in hippocampal neurons blocked by excitatory amino-acid transmitters. *Nature, 347*, 765–767.

Chow, C. C. (1998). Phase-locking in weakly heterogeneous neuronal networks. *Physica D, 118*, 343–370.

Chow, C. C., White, J. A., Ritt, J., & Kopell, N. (1998). Frequency control in synchronized networks of inhibitory neurons. *J. Comp. Neurosci., 5*, 407–420.

Crook, S. M., Ermentrout, G. B., & Bower, J. M. (1998). Spike frequency adaptation affects the synchronization properties of networks of cortical oscillators. *Neural Comp., 10*, 837–854.

Destexhe, A., & Paré, D. (1999). Impact of network activity on the integrative properties of neocortical pyramidal neurons *in vivo*. *J. Neurophysiol., 81*, 1531–1547.

Destexhe, A., Rudolph, M., & Paré, D. (2003). The high-conductance state of neocortical neurons *in vivo*. *Nature Reviews Neurosci., 4*, 739–751.

Diener, F. (1985a). Propriétés asymptotiques des fleuves. *C. R. Acad. Sci. Paris, 302*, 55–58.

Diener, M. (1985b). Détermination et existence des fleuves en dimension 2. *C. R. Acad. Sci. Paris, 301*, 899–902.

Engel, A. K., König, P., Kreiter, A. K., Schillen, T. B., & Singer, W. (1992). Temporal coding in the visual cortex: New vistas on integration in the nervous system. *Trends Neurosci., 15*, 218–226.

Ermentrout, G. B. (1996). Type I membranes, phase resetting curves, and synchrony. *Neural Comp., 8*, 879–1001.

Ermentrout, G. B., & Kopell, N. (1986). Parabolic bursting in an excitable system coupled with a slow oscillation. *SIAM J. Appl. Math, 46*, 233–253.

Ermentrout, G. B., & Kopell, N. (1998). Fine structure of neural spiking and synchronization in the presence of conduction delay. *Proc. Natl. Acad. Sci. USA, 95*, 1259–1264.

Fisahn, A., Pike, F. G., Buhl, E. H., & Paulsen, O. (1998). Cholinergic induction of network oscillations at 40 Hz in the hippocampus *in vitro*. *Nature, 394*, 186–189.

Fries, P., Neuenschwander, S., Engel, A. K., Goebel, R., & Singer, W. (2001). Rapid feature selective neuronal synchronization through correlated latency shifting. *Nature Neurosci., 4*, 194–200.

Fries, P., Roelfsema, P. R., Engel, A. K., König, P., & Singer, W. (1997). Synchronization of oscillatory responses in visual cortex correlates with perception in interocular rivalry. *Proc. Natl. Acad. Sci. USA, 94*, 12699–12704.

Gerstner, W. (2000). Population dynamics of spiking neurons: Fast transients, asynchronous state, and locking. *Neural Comp., 12*, 43–89.

Gerstner, W., & van Hemmen, J. L. (1993). Coherence and incoherence in a globally coupled ensemble of pulse-emitting units. *Phys. Rev. Lett., 71*, 312–315.

Golomb, D., & Rinzel, J. (1993). Dynamics of globally coupled inhibitory neurons with heterogeneity. *Phys. Rev. E, 48*, 4810–4814.

Gray, C. M., & McCormick, D. A. (1996). Chattering cells: Superficial pyramidal neurons contributing to the generation of synchronous oscillations in the visual cortex. *Science, 274*, 109–113.

Gutkin, B. S., & Ermentrout, G. B. (1998). Dynamics of membrane excitability determine interspike interval variability: A link between spike generation mechanisms and cortical spike train statistics. *Neural Comp., 10*, 1047–1065.

Hansel, D., & Mato, G. (2001). Existence and stability of persistent states in large neuronal networks. *Phys. Rev. Lett., 86*, 4175–4178.

Hansel, D., & Mato, G. (2003). Asynchronous states and the emergence of synchrony in large networks of interacting excitatory and inhibitory neurons. *Neural Comp., 15*(1), 1–56.

Hansel, D., Mato, G., & Meunier, G. (1995). Synchrony in excitatory neural networks. *Neural Comp., 7*, 307–337.

Hasselmo, M. E. (1999). Neuromodulation: Acetylcholine and memory consolidation. *Trends in Cognitive Sciences, 3* (9), 351–359.

Hodgkin, A. L. (1948). The local changes associated with repetitive action in a nonmedullated axon. *J. Physiol. (London), 107*, 165–181.

Hoppensteadt, F. C., & Izhikevich, E. M. (1997). *Weakly connected neural networks*. New York: Springer-Verlag.

Izhikevich, E. M. (2000). Neural excitability, spiking and bursting. *Int. J. Bifurcation and Chaos, 10*, 1171–1266.

Knowles, W. D., & Schwartzkroin, P. A. (1981). Local circuit synaptic interactions in hippocampal brain slices. *J. Neurosci., 1*, 318–322.

Kopell, N., & Ermentrout, G. B. (2002). Mechanisms of phase-locking and frequency control in pairs of coupled neural oscillators. In B. Fiedler (Ed.), *Handbook on dynamical systems (Vol. 2: Towards applications* (pp. 3–54). Amsterdam: Elsevier.

Latham, P. E., Richmond, B. J., Nelson, P. G., & Nirenberg, S. (2000). Intrinsic dynamics in neuronal networks. I. Theory. *J. Neurophysiol., 83*, 808–827.

Mirollo, R. E., & Strogatz, S. H. (1990). Synchronization of pulse-coupled biological oscillators. *SIAM J. Appl. Math., 50*, 1645–1662.

Neltner, L., Hansel, D., Mato, G., & Meunier, C. (2000). Synchrony in heterogeneous networks of spiking neurons. *Neural Comput., 12*, 1607–1641.

Olufsen, M., Whittington, M. A., Camperi, M., & Kopell, N. (2003). New functions for the gamma rhythm: Population tuning and preprocessing for the beta rhythm. *J. Comp. Neurosci., 14*, 33–54.

Peskin, C. S. (1975). *Mathematical aspects of heart physiology*. New York: Courant Institute of Mathematical Sciences, New York University.

Pulvermüller, F., Birbaumer, N., Lutzenberger, W., & Mohr, B. (1997). High-frequency brain activity: Its possible role in attention, gestalt processing and language. *Progress in Neurobiology, 52*, 427–445.

Rinzel, J., & Ermentrout, G. B. (1998). Analysis of neural excitability and oscillations. In C. Koch, & I. Segev (Eds.), *Methods in neuronal modeling* (pp. 251–292), Cambridge, MA: MIT Press.

Singer, W. (1999). Neuronal synchrony: A versatile code for the definition of relations. *Neuron, 24*, 49–65.

Singer, W., & Gray, C. M. (1995). Visual feature integration and the temporal correlation hypothesis. *Ann. Rev. Neurosci., 18*, 555–586.

Skinner, F., Kopell, N., & Marder, E. (1994). Mechanisms for oscillation and frequency control in networks of mutually inhibitory relaxation oscillators. *J. Comp. Neurosci., 1*, 69–87.

Slotnick, S. D., Moo, L. R., Kraut, M. A., Lesser, R. P., & Hart, J. (2002). Interactions between thalamic and cortical rhythms during semantic memory recall in human. *Proc. Natl. Acad. Sci. USA, 99*(9), 6440–6443.

Somers, D., & Kopell, N. (1993). Rapid synchronization through fast threshold modulation. *Biol. Cybern., 68*, 393–407.

Storm, J. F. (1989). An afterhyperpolarisation of medium duration in rat hippocampal pyramidal cells. *J. Physiol. (London), 409*, 171–190.

Tallon-Baudry, C., Bertrand, O., Peronnet, C. F., & Pernier, J. (1998). Induced gamma-band activity during the delay of a visual short-term memory task in humans. *J. Neurosci., 18*, 4244–4284.

Tamás, G., Buhl, E. H., Lörincz, A., & Somogyi, P. (2000). Proximally targeted GABAergic synapses and gap junctions synchronize cortical interneurons. *Nature Neurosci., 3*(4), 366–371.

Terman, D., Kopell, N., & Bose, A. (1998). Dynamics of two mutually coupled slow inhibitory neurons. *Physica D, 117*, 241–275.

Tiesinga, P. H. E., Fellous, J.-M., José, J. V., & Sejnowski, T. J. (2001). Computational model of carbachol-induced delta, theta, and gamma oscillations in the hippocampus. *Hippocampus, 11*, 251–274.

Tiitinen, H., Sinkkonen, J., Reinikainen, K., Alho, K., Lavikainen, J., & Naatanen, R. (1993). Selective attention enhances the auditory 40-Hz transient response in humans. *Nature, 364*, 59–60.

Traub, R. D., Bibbig, A., Fisahn, A., LeBeau, F. E. N., Whittington, M. A., & Buhl, E. H. (2000). A model of gamma-frequency network oscillations induced in the rat CA3 region by carbachol *in vitro*. *European J. Neuroci., 12*, 4093–4106.

Traub, R. D., Buhl, E. H., Gloveli, T., & Whittington, M. A. (2003). Fast rhythmic bursting can be induced in layer 2/3 cortical neurons by enhancing persistent Na^+ conductance or by blocking BK channels. *J. Neurophysiol., 89*, 909–921.

Traub, R. D., Kopell, N., Bibbig, A., Buhl, E. H., Lebeau, F. E. N., & Whittington, M. A. (2001). Gap junctions between interneuron dendrites can enhance long-range synchrony of gamma oscillations. *J. Neurosci., 21*, 9478–9486.

Traub, R. D., Whittington, M. A., Colling, S. B., Buzsáki, G., & Jefferys, J. G. R. (1996). Analysis of gamma rhythms in the rat hippocampus *in vitro* and *in vivo*. *J. Physiol. (London), 493*, 471–484.

van Vreeswijk, C. (2000). Analysis of the asynchronous state in networks of strongly coupled oscillators. *Phys. Rev. Lett., 84*, 5110–5113.

van Vreeswijk, C., Abbott, L. F., & Ermentrout, G. B. (1994). When inhibition not excitation synchronizes neural firing. *J. Comp. Neurosci., 1*, 313–321.

van Vreeswijk, C., & Hansel, D. (2001). Patterns of synchrony in neural networks with spike adaptation. *Neural Comp., 13*, 959–992.

Wang, X.-J., & Buzsáki, G. (1996). Gamma oscillation by synaptic inhibition in a hippocampal interneuronal network model. *J. Neurosci., 16*, 6402–6413.

Wang, X.-J., Golomb, D., & Rinzel, J. (1995). Emergent spindle oscillations and intermittent burst firing in a thalamic model: Specific neuronal mechanisms. *Proc. Natl. Acad. Sci. USA, 2*, 5577–5581.

Wang, X.-J., & Rinzel, J. (1992). Alternating and synchronous rhythms in reciprocally inhibitory model neurons. *Neural Comp., 4*, 84–97.

White, J., Chow, C., Ritt, J., Soto-Trevino, C., & Kopell, N. (1998). Synchronization and oscillatory dynamics in heterogeneous, mutually inhibited neurons. *J. Comp. Neurosci., 5*, 5–16.

Whittington, M. A., Stanford, I. M., Colling, S. B., Jefferys, J. G. R., & Traub, R. D. (1997). Spatiotemporal patterns of gamma frequency oscillations tetanically induced in the rat hippocampal slice. *J. Physiol. 502*, 591–607.

Whittington, M. A., Traub, R. D., & Jefferys, J. G. R. (1995). Synchronized oscillations in interneuron networks driven by metabotropic glutamate receptor activation. *Nature, 373*, 612–615.

Whittington, M. A., Traub, R. D., Kopell, N., Ermentrout, B., & Buhl, E. H. (2000). Inhibition-based rhythms: experimental and mathematical observations on network dynamics. *Int. J. Psychophysiol., 38*, 315–336.

Received February 17, 2004; accepted July 27, 2004.